ADVANCED FUNCTIONAL MATERIALS
www.afm-journal.de

An Ultrahydrating Polymer that Protects Protein Therapeutics and RNA-Lipid Nanoparticles Against Freezing, Heat and Lyophilization Stress

Anna Herrmann, Srinivas Abbina, Nuthan Vikas Bathula, Peyman Malek Mohammadi Nouri, Irina Chafeeva, Iren Constantinescu, Emaan Abbasi, Usama Abbasi, Matthew Drayton, Haiming Daniel Luo, Haisle Moon, Arshdeep Gill, Yu Xi, Allan K. Bertram, Caigan Du, Rainer Haag, Anna K. Blakney, and Jayachandran N. Kizhakkedathu**

RNA and protein-based therapeutics constitute almost half of recent drug approvals and receive considerable attention within biotechnology industries. Ensuring their stability and longevity in the context of heat, freezing, and lyophilization processes are paramount to a successful deployment. However, the advancement of formulations designed to achieve this goal is still in its nascent phase. To address these challenges, a new class of semi-dendritic hydrophilic polymer with extended linear units is reported, which showcase very high hydration. These novel polymers demonstrated exceptional efficacy in preserving messenger RNA- (mRNA-) and self-amplifying RNA- (saRNA-) lipid nanoparticles during freezing and lyophilization. Additionally, they have been found to protect therapeutic proteins against external stressors such as freezing, heat, and lyophilization. These polymers are non-toxic, which enables their utilization at high concentrations and eliminates the requirement for removal prior to administration. It is found that their unique topology contributes to the high hydration. These excipients are anticipated to create new prospects in biotechnology, food science, and cryopreservation.

1. Introduction

Biotherapeutics, including recombinant therapeutic proteins, hormones, monoclonal antibodies, enzymes, and growth factors represent a major portion of the current pharmaceutical market.[1,2] Following the expedited and effective development of messenger RNA-based lipid nanoparticle (mRNA-LNP) vaccines in response to the emergence of SARS-CoV-2, there has been even greater momentum in the field of genetic medicine.[3,4] Established as a vaccine against COVID19 and RSV, the mRNA-LNP technology is now being explored as a potential modality for future advancements in cancer treatment, genetic disorders, other infectious diseases, and CRISPR/Cas technologies which will likely increase the prevalence of LNPs in the field of gene medicine.[5–8]

A. Herrmann, S. Abbina, P. M. M. Nouri, I. Chafeeva, I. Constantinescu, U. Abbasi, M. Drayton, H. D. Luo, H. Moon, A. Gill, J. N. Kizhakkedathu
Center for Blood Research
Life Sciences Institute
The University of British Columbia
Vancouver, BC V6T 1Z3, Canada
E-mail: jay@pathology.ubc.ca

A. Herrmann, S. Abbina, P. M. M. Nouri, I. Chafeeva, I. Constantinescu, E. Abbasi, U. Abbasi, M. Drayton, H. Moon, J. N. Kizhakkedathu
Department of Pathology and Laboratory Medicine
The University of British Columbia
Vancouver, BC V6T 1Z3, Canada

The ORCID identification number(s) for the author(s) of this article can be found under https://doi.org/10.1002/adfm.202406878

DOI: 10.1002/adfm.202406878

N. V. Bathula, A. K. Blakney, J. N. Kizhakkedathu
The School of Biomedical Engineering
The University of British Columbia
Vancouver, BC V6T 1Z3, Canada
E-mail: anna.blakney@msl.ubc.ca

N. V. Bathula, A. K. Blakney
Michael Smith Laboratories
The University of British Columbia
Vancouver, BC V6T 1Z4, Canada

H. D. Luo, A. Gill, Y. Xi, A. K. Bertram, J. N. Kizhakkedathu
Department of Chemistry
The University of British Columbia
Vancouver, BC V6T 1Z3, Canada

C. Du
Department of Urological Sciences
University of British Columbia
Vancouver, BC V5Z 1M9, Canada

R. Haag
Institute of Chemistry and Biochemistry
Freie Universität Berlin
Takustrasse 3, 14195 Berlin, Germany

A major challenge to be tackled in this research field is the requirement for storage of active formulations at ultra-low temperatures.[9] The LNPs as the crucial carrier system to preserve the activity of nucleic acids, however, can burst, aggregate, or collapse during freeze-thaw cycles, meaning they require appropriate stabilization, preservation, and transportation protocols. Similarly, most protein-based biotherapeutic agents lose their activity upon exposure to external stimuli, such as temperature fluctuations, light, desiccation, pH change, osmotic change, mechanical agitation, and hydrophobic surface interactions.[10,11] Currently, these pharmaceuticals are stored and preserved in formulations using excipients, such as amino acids, osmolytes, carbohydrates, and natural polymers;[12] however, these excipients suffer from low efficiency, immunogenicity, high osmolarity, or interference with biological function.[13,14] Since the inception of LNPs, enhancing their storage and stability has been a continuous priority, yet much about their structure remains to be elucidated. While significant strides have been made in understanding biotherapeutics and their stabilization,[15–17] many challenges remain. The challenges faced in the preservation of biotherapeutics and LNPs include toxicity (e.g., DMSO, glycerol) and difficulty in removing very high concentrations of cryoprotectants. Recently, there has been exploration into using macromolecule-based excipients, such as polymers, hydrogels, and zeolites, for storing protein-based biotherapeutics.[15–19] However, their biocompatibility and safety profiles remain undefined. While some carbohydrate-based systems have been investigated for preserving lipid nanoparticle (LNP)-based vaccines, macromolecular excipients have received less attention. Additionally, there is a lack of clinically viable lyophilization buffers for safely storing and transporting LNP-based therapeutics and vaccines. Thus, new (cryo)preserving molecules that are highly biocompatible and non-immunogenic are needed, while still delivering optimal performance to advance this important research field.

Molecules possessing cavities or pockets that can accommodate water molecules exhibit distinct macroscopic properties, such as slowing ice crystal growth, non-colligative depression of freezing point, and inimitable dynamic structural, chemical, and surface properties.[20–23] Owing to their specific interactions with water, hydrated materials have been widely explored as stabilizing agents for proteins, enzymes,[24] food ingredients,[25] growth factors,[26] skin hydrating products,[27] and for cryopreservation of LNPs.[28] Such studies are exemplified by excipients that are Generally Recognized as Safe (GRAS) by the FDA, such as disaccharides trehalose and sucrose[29] or polymers such as polyvinyl alcohol[30] and hyaluronic acid.[27] Despite the progress made in this field, our understanding of the design principles behind highly hydrating macromolecules remains limited.[20,31]

Herein, we report the development of a class of semi-dendritic ultra-hydrating polymers, hyperbranched poly (3-(oxiran-2-ylmethoxy) propane-1,2-diols (HPODs), that are highly effective in stabilizing diverse biotherapeutics, including mRNA-LNP, saRNA-LNP, proteins, enzymes, and antibodies against external stresses such as freezing, heating, and lyophilization compared to the current gold standards used in academia as well as in industry. These branched polymers were well tolerated in vivo at high concentrations, eliminating the need to be removed prior to administration. Moreover, we demonstrate the significance of polymer topology in determining their exceptional hydration properties, thereby establishing an additional design criterion alongside chemical composition.

2. Results

2.1. Design and Development of Semi-Dendritic Highly Hydrated Polymers

To achieve a highly hydrated structure for the preservation of biotherapeutics, our design strategy involved the combination of a hydrophilic polyether-polyol based backbone, with an optimized topology that facilitates the accommodation of more unfreezable water. The formation of a hydrogen-bond network amongst water molecules is directly associated with the crystallization during freezing. Therefore, molecules or polymers that can disrupt the hydrogen bonds between water molecules may have the potential to prevent the growth and formation of ice.[21,31] Considering the fact that extensive hydrogen-bonding networks and the presence of multiple water-binding functional groups may provide highly hydrated macromolecules, we developed a monomer 3-(oxiran-2-ylmethoxy)propane-1,2-diol (OPD) (glycerol glycidol monoether) (Figure S1, Supporting Information). This monomer can be polymerized through ring opening multi-branching polymerization (ROMBP) to create a dendritic polyether backbone with numerous hydroxyl groups. A branched polymer structure was chosen due to its potential advantages, including limited inter-chain interaction, low intrinsic viscosity, and high biocompatibility as opposed to the linear structure.[32–34] The monomer was synthesized by epoxidation of 3-(allyloxy)propane-1,2-diol in decent yields (60–70%) and characterized by different spectroscopic techniques (Figures S1–S4, Supporting Information). Together with ^{1}H, ^{13}C, and HSQC NMR and mass spectrometry, the structure of the OPD monomer was confirmed.

By employing anionic ROMBP,[35] a small library of hyperbranched poly (3-(oxiran-2-ylmethoxy) propane-1,2-diol (HPOD) polymers were synthesized with molecular weights ranging from 640 to 11, 500 Da (see **Figure 1**; Figures S5–S7, Supporting Information) by changing the monomer to initiator ratios, varying base and using emulsification agents (detailed in the supplementary information). A key challenge faced was the dehydration of the monomer for polymerization. A considerable amount of bound water was found to be associated with OPD monomer (7–18 wt% water based on thermogravimetry analysis), which necessitates very stringent dehydration protocols before attempting ROMBP. The obtained honey-like HPOD polymers were highly hygroscopic and water-soluble.

The structural and physical characterization of HPOD polymers were performed using multiple analytical methods. The absolute molecular weights of the HPODs ranged from 640 to 11,500 Da (Figure 1b; Figure S7, Supporting Information) obtained by GPC-MALS. The hydrodynamic sizes of HPODs are in the range of 2–4.8 nm as measured by pulse field gradient NMR spectroscopy, and as expected there is a modest increase in the hydrodynamic size with the increase in molecular weight (Figure 1b; Table S2 and Figure S8, Supporting Information). HPODs also showed low intrinsic viscosities (η) in water in the range of 4.2-6.5 mL/g (Figure 1b), which is low compared to linear polymers, such as Polyethylene glycol (PEG),

a)

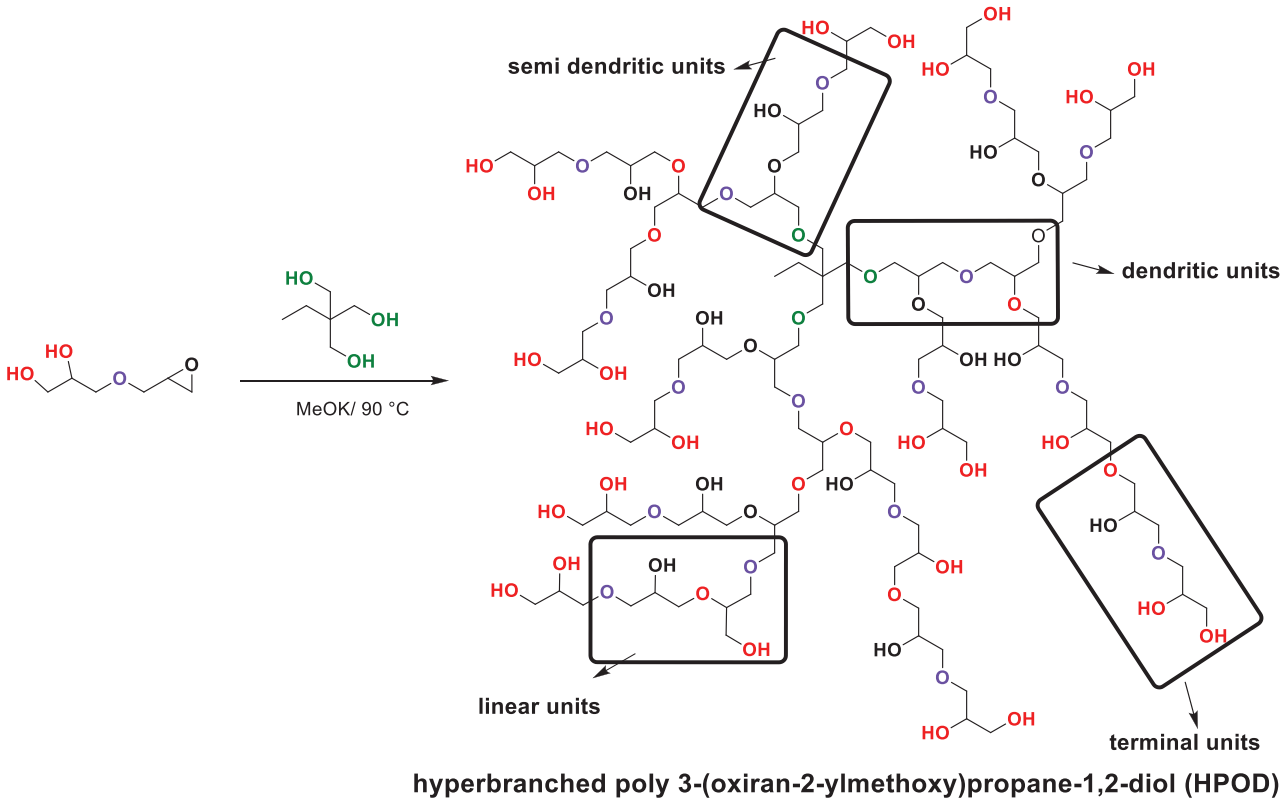

hyperbranched poly 3-(oxiran-2-ylmethoxy)propane-1,2-diol (HPOD)

b)

Excipient	M_n(Da)	Đ	hydration number/monomer	hydrodynamic size (nm)	intrinsic viscosity (η), mL/g
HPOD-**1**	640	1.10	26.9± 1.1	2.0 ± 0.42	-
HPOD-**2**	1090	1.10	25.4± 2.5	2.0 ± 0.10	4.2
HPOD-**3**	2300	1.20	17.9 ± 1.0	4.2 ± 0.24	4.8
HPOD-**4**	4000	1.60	15.5 ± 0.20	3.0 ± 0.14	5.3
HPOD-**5**	11500	1.30	14.7 ± 1.0	4.8 ± 0.16	6.5
Trehalose	342	-	22.3	0.9[41]	-

Figure 1. Synthesis and characterization of hyperbranched poly 3-(oxiran-2-ylmethoxy)propane-1,2-diol (HPOD). a) Scheme of a representative synthetic route for HPOD by anionic ring opening multibranching polymerization (ROMBP) of 3-(oxiran-2-ylmethoxy)propane-1,2-diol (OPD). The possible different structural linkages within HPOD are shown (inserts). b) Absolute molecular weight and intrinsic viscosity of the HPODs were determined by triple detection gel permeation chromatography (GPC) analysis (multi-angle static light scattering (MALS), refractive index detector, and viscometer detectors). HPODs are abundant with bound water, and the hydration is determined by measuring the fusion enthalpy of polymer solution by differential scanning calorimetry. The hydrodynamic size ($2R_h$) of the HPODs is measured by Stokes–Einstein equation, $R_h = kBT/6\pi\eta Dt$; the translational diffusion coefficient (Dt) is determined using pulse-field gradient nuclear magnetic spectroscopy.

polyvinylpyyrolidine (PVP), or polyvinylalcohol (PVA) but similar to that of globular proteins.[34] There is a slight increase in intrinsic viscosities of HPODs (Figure 1b) with molecular weight. NMR (^{1}H, ^{13}C, and DEPT), Matrix-assisted laser desorption/ionization time-of-flight mass spectrometry (MALDI-ToF), Electrospray Ionization Mass Spectrometry (ESI-MS) and were used for the structural characterization of the HPODs (**Figure 2** and Supplementary information).

In ^{1}H NMR, the protons of the polymer backbone were observed between 3–4 ppm, and the initiator, trimethylolpropane, proton peaks were observed at 1–2 ppm (Figure S5, Supporting Information). A set of well-resolved peaks for different carbons

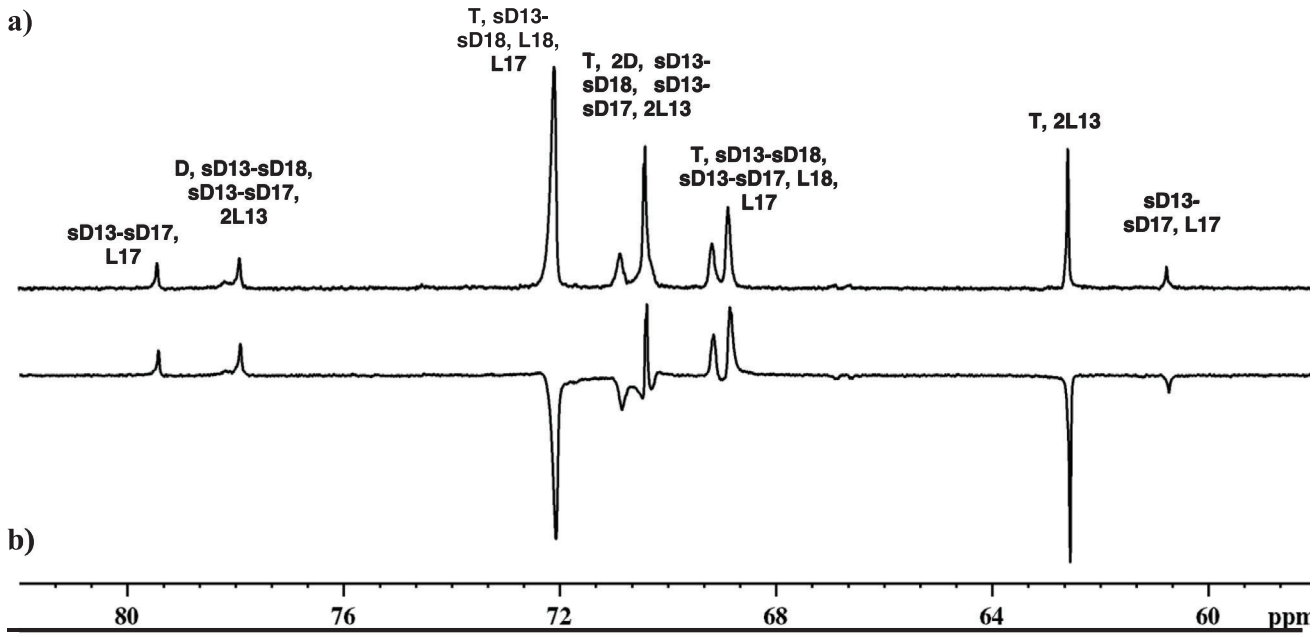

Polymer	sD13-sD17, L17	D, sD13-sD18, sD13-sD17, 2L13	T, sD13-sD18, L18, L17	T, 2D, sD13-sD18, sD13-sD17, 2L13	T, sD13-sD18, sD13-sD17, L18, L17	T, 2L13	sD13-sD17, L17	DB
HPOD-**1**	1	0.68	25.61	16.39	10.24	8.77	0.87	23
HPOD-**2**	1	1.48	28.54	15.21	13.36	7.82	0.92	29
HPOD-**3**	1	2.24	23.46	17	12.23	5.91	0.84	37
HPOD-**4**	1	3.02	23.66	17.66	12.19	5.61	0.78	42
HPOD-**5**	1	4.86	29.24	24.88	15.73	7.02	0.96	46

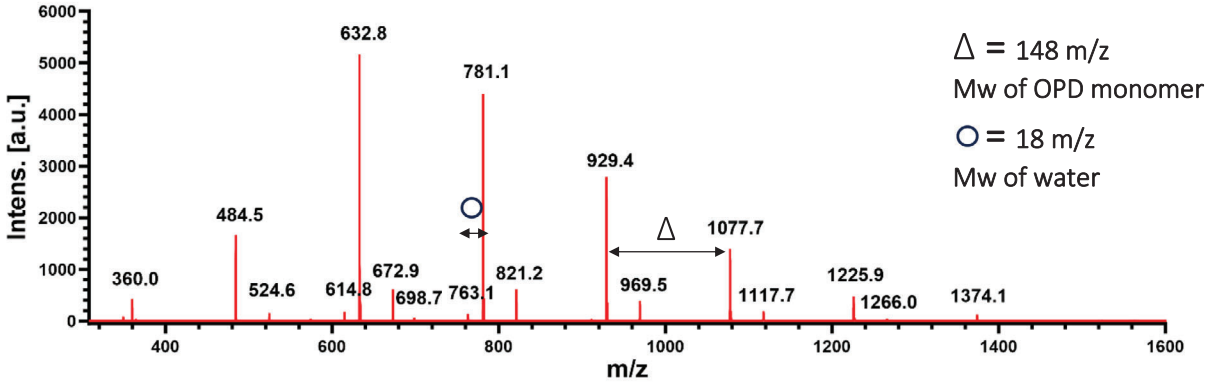

Figure 2. Structural analysis to determine the degree of branching of HPODs. a) ^{13}C Inverse gated and b) DEPT NMR spectral analysis to identify the -CH (up) and – CH_2 carbons with assigned structural units. The ratio between the different branching units of the HPODs is used to calculate their degree of branching (DB) which was calculated using the equation, DB = (2D+sD)/(2D+(4/3)sD+2/3(L)). c) MALDI-ToF spectra of HPOD-2 having multiples of 148 Da as main peaks which is equivalent to the molecular weight of the OPD monomer and peaks at a difference of 18 m/z indicating water adducts.

were observed between 60–80 ppm on ^{13}C NMR spectrum (Figure 2a; Figure S6, Supporting Information). To elucidate additional structural information of HPOD polymers, the degree of branching (DB) of HPODs was measured using inverse-gated ^{13}C NMR (Figure 2a). As it is an AB_3 monomer, DB was calculated using the equation, DB = 2D+*s*D/(2D+(4/3)sD+2/3L)).[35,36] Four structural configurations of HPODs were labeled as perfect dendritic (D), semi dendritic (*s*D), linear (L), and terminal units (T). The possible structural linkages in these configurations were described as D_{13}-D_{17}-D_{18} in dendritic, L_{13}, L_{17}, and L_{18} in linear configuration, and sD_{13}-sD_{17}, sD_{13}-sD_{18} in semi dendritic units and their intensities were analyzed using ^{13}C inverse-gated and DEPT NMRs (Figure 2; Figures S9 and S11 (Supporting Information), see also the additional Excel file in supplementary information). Although different proportions of these structural configurations (D, *s*D, L, and T) are theoretically expected, we could not identify the proportions at the given NMR experimental conditions and thus, adopted the theoretical approximations to derive the DB of the polymers. The DB increased with the molecular weight of the polymer; HPOD-**1** (M_n-640 Da) had 23% branching and DB reached up to 46% for HPOD-**5** (M_n-11,500 Da) (Figure 2c).

Additional structural information has been obtained from MALDI-ToF mass spectrometry,[37] including the monomer incorporation, presence of initiator unit, and the incorporation of counter ions. The MALDI-ToF spectra of HPOD-1 and HPOD-2 are given in Figure 2d and in Figure S12 (Supporting Information). The mass difference between the peaks represents precisely the molecular mass of OPD monomer (148 m/z) in both spectra suggesting that OPD monomer is incorporated within the polymer and the mass of the repeating unit is 148 Da. The MALDI spectra reveal additional information. Each of the peaks consists of either H+ or Na+ as a cation counter ion adduct and each peak consists of the sum of the mass of the core unit 1,1,1-tris(hydroxymethyl)propane (134 m/z) (see Table S3, Supporting Information for the analyses of different peaks). An intriguing observation is that each peak of HPOD in the spectra has 2–4 bound water molecules depending on the m/z value of the peak. For example, in the case of HPOD-2, higher m/z peaks do have 4 water molecules in comparison to peaks at lower m/z values. Detailed analyses of the peaks of MALDI spectra for both polymers and the calculation is given in Figure S12 and Table S3 (Supporting Information). Similar water adducts were reported for the MALDI spectra of sugar molecules,[38] suggesting that HPOD polymers are highly hydrated as hypothesized and are quite different from other branched polyether polyols.[37] In addition, ESI mass spectra of HPOD (Figure S12, Supporting Information) show monomer and initiator incorporation, difference in repeating unit, and hydration. These features differentiate the HPOD structure from well-studied hyperbranched polyglycerol (HPG),[32,35] which are prepared by anionic ROMBP of glycidol, an AB_2 type monomer and polyglycerol dendrimer (PGD)[39] (discussed in later section).

2.2. Hydration Characteristics of the HPODs

Important structural features of HPODs are their branched polyether structure with significant linear structure content along with dendritic units with low degree of branching and with an abundance of both primary and secondary hydroxyl groups. Together these properties are anticipated to generate a highly hydrating structure. Thus, we investigated the hydration characteristics of HPODs. The number of bound unfrozen water molecules associated with HPOD is determined from the hydration enthalpy of aqueous solutions by differential scanning calorimetry (Figure S13a, Supporting Information) and results are displayed per monomer in Figure 1b.[40] The hydration levels vary depending on the molecular weight of the HPODs, with hydration numbers ranging from 15 to 27 water molecules per monomer unit compared to ≈22 for trehalose[41] and ≈4 for PEG.[42] Interestingly, lower molecular weights provided higher hydration values, which is most likely attributed to their less branched nature and thus more accessible hydroxyl groups throughout the polymer structure. When compared to trehalose, a disaccharide, which is the benchmark in the field, HPOD-**1** and HPOD-**2** demonstrated even greater amounts of water per monomer unit.[41]

2.3. Cryopreservation of RNA-LNPs in the Presence of HPOD Excipients

The use of lipid nanoparticle (LNP) carrier systems is essential for delivering charged nucleic acid cargo such as small interfering RNA (siRNA),[43] messenger RNA (mRNA),[44] or self-amplifying RNA (saRNA)[45] into cells, where it can release its cargo to regulate gene expression or enable translation. While significant efforts have been focused on enhancing the efficacy and stability of these formulations in vivo, there is still much to be explored and optimized in terms of storage conditions and particle preservation during storage.[46] To ensure that the LNP remains intact during storage at ultra-low temperatures, which are necessary for preserving RNA functionality, excipients are added to the formulation to retain the physicochemical properties of the delivery vehicle.[47,48] While various studies have focused on enhancing LNP stability and efficacy through lipid component and formulation parameter optimization, failure to maintain these improvements during storage, distribution, and reconstitution may render the formulation noncompliant with the necessary standards.[49] The approved mRNA-based vaccine formulations from Comirnaty (BioNTech/Pfizer) and Spikevax (Moderna) use sucrose for preservation at 20% w/v in PBS and 8% w/v in Tris, respectively, which is considered safe.[50] Comirnaty is reported stable when stored at −70 °C for up to 6 months, and Spikevax is stored at −20 for up to 6 months. Sucrose is a highly osmotic compound that can cause damage to cells and tissue and thus, limits its use at high concentrations. Low concentrations, however, can lead to inadequate preservation, necessitating the need for alternatives possessing improved biocompatibility and lower osmolarity.

Due to their highly hydrated nature, we hypothesized that HPOD might be an excellent candidate to be used for cryoprotecting RNA-LNP formulations. Thus, we chose mRNA encoding for enhanced green fluorescent protein (EGFP) encapsulated into LNPs (mRNA-LNP) and prepared a series of formulations by adding different HPODs as excipients and compared them to an unpreserved control in the buffer. To emulate the cold-storage condition of mRNA-LNP formulations, we exposed the

formulations to a freeze-thaw cycle at −70 °C and determined the physicochemical properties after thawing the next day. We then compared them to those of freshly prepared mRNA-LNPs that never went through a freeze-thaw cycle. We considered mRNA-LNPs as fresh if they were used within one week and referred to their size, polydispersity index (PDI), encapsulation efficiency (EE)%, and % transfected compared to the original. Initial screening of the HPOD library at different concentrations (see Figure S15, Supporting Information) was performed to identify the best preservation conditions and compared to FDA approved excipients sucrose and trehalose at the same concentration. Initially, we looked at the size and PDI by Dynamic light scattering (DLS), and determined the encapsulation efficiency (EE%) by the Ribogreen assay (see **Figure** 3a–c). A small increase in size and PDI was seen when compared to the original values of mRNA-LNPs that never went through a freeze-thaw cycle; the size increase was least pronounced for HPOD-**2** and HPOD-**5**, meaning these polymers performed as well as FDA-approved sucrose formulations. Interestingly, we observed an increase in size and PDI prior to freezing (see Figure S16, Supporting Information). Thus, we believe it is more likely attributed to the additives interacting with the LNP corona, thereby increasing the hydrodynamic radius and not by altering the actual LNP structure. As depicted in Figure 3c,d, the increase in size is not associated with any loss in EE% or transfectability for all HPODs suggesting that all mRNA molecules were still encapsulated within the LNPs after going through a freeze-thaw cycle. This was confirmed by determining the RNA integrity after a freeze-thaw cycle, showing that HPOD as excipient was able to preserve the RNA (Figure 3e).

Next, we used cryo-preserved LNPs to transfect both CHO and HeLa cells (see Figure 3d; Figure S17, Supporting Information). The cells were transfected for 24 h and then subjected to analysis by flow cytometry; values were compared to freshly prepared mRNA-LNP. Both, high and low molecular weight polymers (HPOD-**5** and HPOD-**2**) maintained the transfectability. The data showed superior performance to HPOD-**4** and trehalose and were equally effective as sucrose at high concentrations.[51] The number of freeze-thaw cycles should be minimized to ensure the stability and integrity of formulations. However, it is desirable for an excipient to provide protection to the formulation for more than a single cycle. Therefore, we carried out a study wherein the formulation underwent three complete freeze-thaw cycles. Notably, despite the exposure to multiple cycles, the formulations demonstrated consistent and sustained transfectability (see Figure S18, Supporting Information). Additionally, confocal microscopy images of transfected HeLa cells clearly demonstrate that mRNA-LNP complexes cryopreserved with HPOD-**5** exhibit consistent and uniform transfection, as evident by sustained EGFP expression in both pre-freezing and post-freezing (see Figure 3f). Conversely, unpreserved mRNA-LNPs exhibit a significant decline in transfection efficiency.

Encouraged by these findings, we proceeded with the use of HPOD-5 and evaluated its in vivo transfection capabilities following intramuscular injection (*i.m.*). Thus, we prepared mRNA encoding for firefly luciferase (fLuc) encapsulated into LNPs. After storage at 70° C both the unpreserved and cryopreserved formulations were injected into Balb/c mice and compared with freshly prepared mRNA-LNPs as reference (see Figure 3g). Luminescence was recorded on Day 2 and results are shown in Figure 3h. The HPOD-**5** preserved LNPs showed no significant difference in luminescence compared to freshly prepared LNPs, meaning that no loss of transfectability was observed during the freeze-thaw cycle.

Further, we evaluated the preservation of self-amplifying RNA based LNPs (saRNA-LNP). Unlike traditional mRNA, which only carries the code for one protein, saRNA contains the code for both the target protein and an RNA replicase enzyme, which can create multiple copies of the mRNA within the cell.[52] This leads to a much higher level of protein production, making saRNA a potentially powerful tool for gene therapy. The much longer chain length of saRNAs (≈10 000 nt) compared to mRNAs (≈1,000 nt) makes them much more prone to degradation and thus, cold-storage and careful preservation is of utmost importance. To demonstrate the scope of applicability we next investigated the preservation of saRNA-LNP encoding for fLuc. After confirming the preservation of the physicochemical properties by HPOD in the case of saRNA-LNPs (see Figure S20, Supporting Information), we performed studies of both preserved and unpreserved saRNA-LNPs in Balb/c mice. Figure 3i shows the results imaged at Day 7 post injection. Again, HPOD-**5** fully preserved the transfectability with no significant difference to freshly prepared saRNA-LNP. With the additional advantages of low osmolarity (5.3 ± 2 mOsm for HPOD-**4** versus 31.7 ± 2 mOsm for sucrose, at 10 mg mL^{-1}), being highly biocompatible (as discussed later), and having synthetic control, our highly hydrated excipient demonstrated its potential as a new cryoprotectant for LNP-based gene delivery.

2.4. Lyophilization of mRNA-LNPs

Lyophilization is an excellent preservation method compared to freezing, particularly for products that require long-term stability and preservation of their original structure and properties.[53] It can extend the shelf life of products and reduce storage and shipping costs because lyophilized products are lighter and take up less space than frozen products. The removal of water minimizes degradation of the product during storage and handling as water is the key factor for product degradation of biologically active samples; it can facilitate chemical reactions such as pH changes, osmotic changes, hydrolysis or oxidation, and promote enzymatic degradation. Thus, we screened a small HPOD-library for their efficacy as lyoprotectants and identified the high molecular weight HPOD-**5** as the best candidate based on size preservation and EE%. As shown in Figure 3, HPOD-**5** worked as an excellent lyo-protectant for mRNA-LNPs. The mRNA-LNPs are lyophilized overnight, and reconstituted in water, and size, PDI, EE%, and transfection efficiency in HeLa cells were determined and compared to the values of freshly prepared mRNA-LNP (see **Figure** 4a–d and CHO cell transfection in Figure S17, Supporting Information). In all cases, a significant size increase was observed when compared to the freshly prepared mRNA-LNP. This is a known effect in literature and is thought to be attributed to a reorganization of the lipids upon reconstitution in water, however, the process is still not fully understood.[54,55] Regardless of the size increase, the PDI, EE%, and transfection in both HeLa and CHO cells are fully preserved by HPOD-**5**, to a similar or better extent than sucrose.

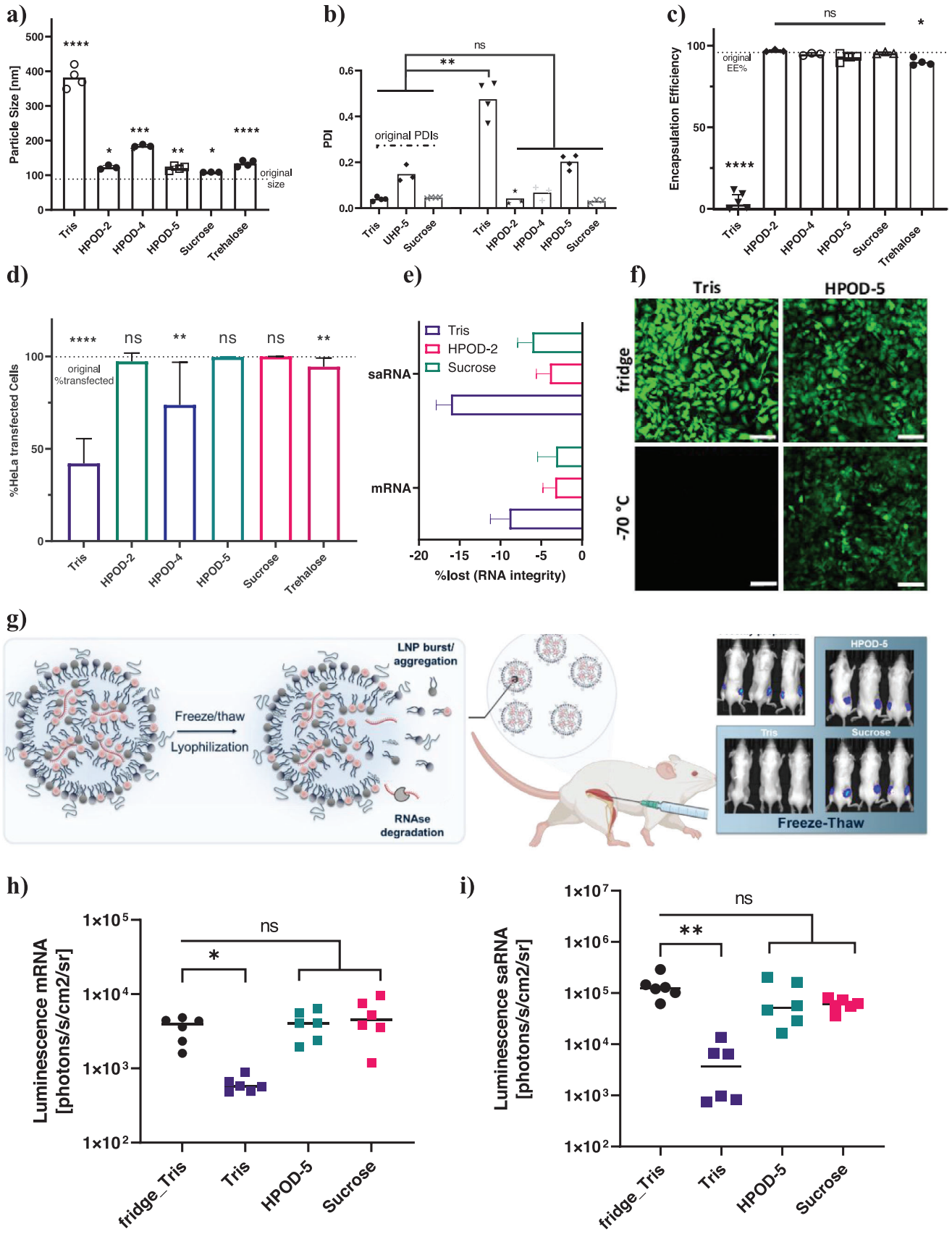

We then studied the in vivo performance of lyophilized formulations, and the results are shown in Figure 4e. The luminescence after *i.m.* injection of mRNA-LNPs was lower after lyophilization for all samples compared to the signal of freshly prepared mRNA-LNPs. The signal for HPOD5 preserved mRNA-LNPs was as high as that of sucrose and the results show that the preserved LNPs had sufficient functional mRNA present. In order to investigate if there is a synergistic or additive effect of sucrose and HPOD we prepared one formulation with a 1:1 mix of sucrose and polymer whereby the final excipient concentration remained constant. The measured luminescence was slightly better however not significant when compared to sucrose or HPOD alone, indicating that the sugar and polymer may preserve LNPs in a cooperative fashion. Further studies are needed to elucidate if the advantages gained from dry storage conditions would make up for the loss in transfection efficacy. Additionally, there are more factors to consider when lyophilizing, such as the optimization of the reconstitution buffer, storage of the lyophilized product, or the lyophilization method. To fully exploit the potential of our polymer, further investigations are necessary to evaluate its long-term stability under various storage conditions, including room temperature, −20 and −70 °C.

2.5. Protein Stabilization and Excipient Activity of HPODs

Next, we investigated whether the highly hydrated HPODs can preserve other biotherapeutics such as proteins which are often very sensitive to different external stresses and are prone to chemical and physical degradation.[11,56] We chose four industrially and therapeutically relevant proteins in this study; lysozyme, insulin, β-galactosidase, and an anti-blood group A antibody. The activities of these proteins after exposing them to external stresses such as freezing, heat, and lyophilization (**Figure 5**; Figure S21 and S22, Supporting Information) in comparison to the current industry standards were measured. Our library screening studies for the stabilization of lysozyme from heat shock (60 °C for 30 min) show the activity of lysozyme after being stabilized with different HPODs in comparison to trehalose as GRAS listed excipient (see Figure 5a) at an identical concentration (50 mg mL^{-1}). HPOD-**4** and HPOD-**3** preserved the activity almost similar to the native protein demonstrating its excellent stabilization ability in comparison to best-known stabilizer trehalose. The low molecular weight HPOD-**1** was not as effective as the other HPODs. Further, HPODs showed superior stabilization ability in comparison to different hydrophilic polymers, including PEG, PDMA, polyglycerol, and dextran (Figure S21, Supporting Information). We then investigated the concentration-dependent activity for HPOD, whereby HPOD-**4** exhibited superior performance in comparison to trehalose (0.1, 0.5, 1, and 50 mg mL^{-1}) (Figure 5b). HPOD-**4** is effective even at 0.5 mg mL^{-1} whereas trehalose did not show any concentration dependency.

We next investigated the stabilization activity of HPODs against aggregation of insulin upon heating in comparison to other established excipients (Figure 5c; Figure S22, Supporting Information). Insulin was heated at 60 °C for 48 h in the presence of different stabilization agents (final concentration was 0.5 mM) and measured the amount/proportion of intact insulin using a thioflavin T based fluorescence assay. HPODs showed significantly better performance in inhibiting fibril formation compared to trehalose, PEG, and proline; no molecular weight dependence is observed for HPODs. Finally, we investigated the stabilization of proteins upon lyophilization and freeze-thaw induced stress as it is known to damage the structure of the proteins severely. β-Galactosidase is an enzyme with significant industrial relevance, however, it denatures upon lyophilization.[57] The activity of β-galactosidase after exposure to multiple lyophilization cycles in the presence and absence of HPOD is measured. Trehalose was used as a control (Figure 5d).[58] Both HPOD and trehalose are effective in stabilization of β-galactosidase against lyophilization stress. However, HPOD-**2** showed improved performance at low concentrations compared to trehalose. With this, we were further interested in evaluating the efficiency of HPODs for preserving the activity of antibodies upon repeated freeze-thaw cycles. Antibodies are usually stored at 20 °C; however, the retention of therapeutic activity of the antibodies after repeated thawing is a humongous challenge in both academic as well as in industrial settings. We chose an anti-blood group A antibody (anti-A antibody) as a model antibody and measured its activity for binding human blood group A (monofucosyl and difucosyl A antigens) on red blood cells (RBCs) after three repeated freeze-thaw cycles (−20 °C to RT, each cycle is repeated every 24 h) using flow cytometry. A fresh antibody aliquot that never went through freeze-thaw cycles was used as a control (Figure 5e). HPOD-**2** and HPOD-**4** demonstrated the preservation of antibody function and exhibited superior performance compared to trehalose on days 1 and 2. While no statistical difference was observed among the stabilizing agents on day 3, it is evident that HPOD-**2** exhibited activity similar to that of the fresh antibody.

Collectively, these findings demonstrate that HPODs are promising stabilizing excipients for both industrially relevant and therapeutic proteins. HPODs effectively protected these

Figure 3. Cryopreservation of RNA-LNP using HPODs. a–d) Freshly prepared mRNA-LNP were mixed with cryopreservation agents (HPOD, sucrose, trehalose, or buffer only (Tris buffer, 20 mM, pH 7)) and stored at 70 C overnight. After thawing, HPODs showed significant improvement compared to unpreserved control in the conservation of a) size, b) PDI, c) EE%, and d) transfection in HeLa cells. Data was reported for at least three independent experiments, $^{*}p < 0.1$, $^{**}p<0.01$, $^{***}p < 0.001$ $^{****}p < 0.0001$, versus original size, PDI, EE%, and %transfected cells, respectively). e) Both, mRNA and saRNA integrity within the LNPs, measured after one freeze-thaw cycle on a bioanalyzer. %lost is the loss in integrity when compared to the integrity of freshly prepared fridge samples. f) Confocal microscopy images of HeLa cells transfected with mRNA-LNPs encoding for enhanced green fluorescent protein, which were either preserved by HPOD-**5** or remained unpreserved (Tris, 20 mM, pH 7) during cryostorage at 70 °C. The top column represents freshly prepared mRNA-LNP that were just mixed and stored in the fridge. The scale bar is 100 µm. g) Schematic of potential degradation processes during freezing and lyophilization of mRNA-LNP and their *i.m.* injection into mice after cryostorage. h) Quantification of luminescence recorded in Balb/c mice 2d after *i.m.* injection of mRNA-LNP encoding for fLuc. Results are shown as mean of $n = 6$ injections into 3 mice ($^{*}p < 0.1$). **i**) shows the results 7 d after saRNA-LNP injection after they went through a freeze-thaw cycle (70 °C). Results are compared to freshly prepared samples (fridge_Tris) and are shown as mean of $n = 6$ injections into 3 mice ($^{**}p < 0.01$).

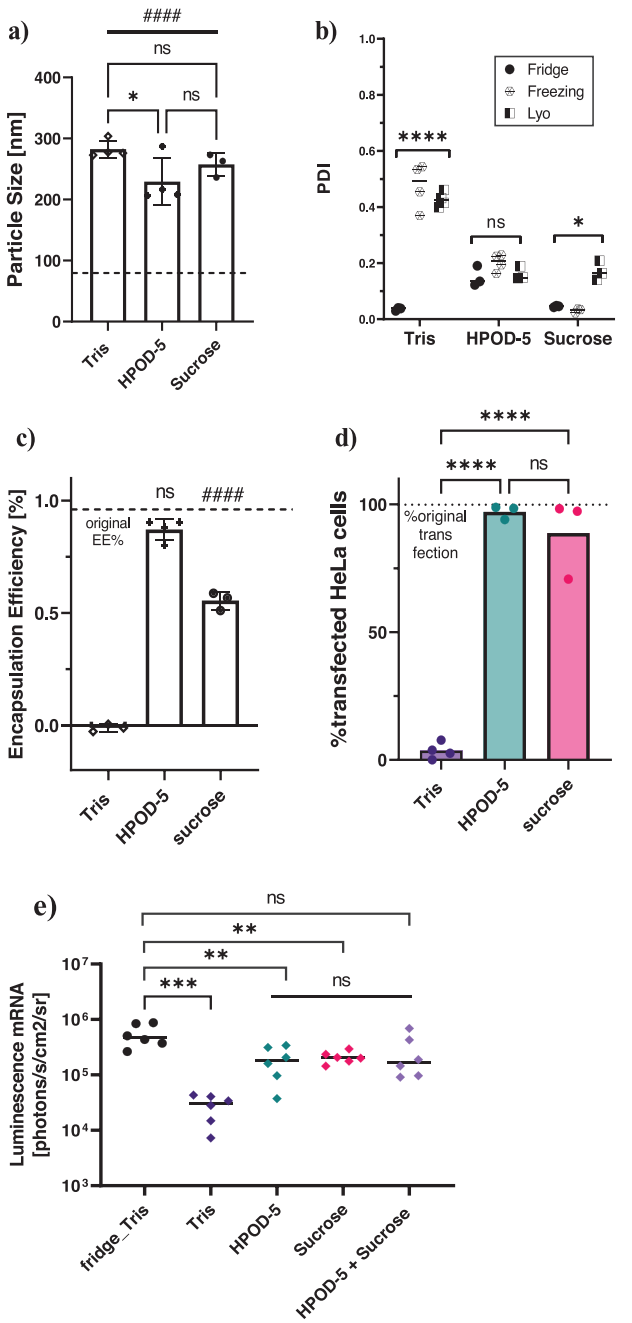

Figure 4. Preservation during lyophilization of mRNA-LNP using HPOD. Freshly prepared mRNA-LNP were mixed with preservation agents HPOD-5 and sucrose or just buffer (Tris, 20 mM, pH 7) and lyophilized overnight. After reconstitution in water a) particle size, b) PDI, and c) encapsulation efficiency were determined. All samples showed a significant size increase ($^{\#\#\#\#}p < 0.0001$ versus original size) but PDI and EE% remained the same (ns) for HPOD-5, outperforming sucrose ($^{*}p < 0.1$ versus fridge PDI and $^{\#\#\#\#}p < 0.0001$ versus original EE%). d) Transfection in HeLa cells showed full preservation of transfectability by both HPOD-5 and sucrose. Data was reported for at least three independent experiments. e) Quantification of luminescence recorded in Balb/c mice 1 d after i.m. injection of mRNA-LNP encoding for fLuc. Results are shown as mean of $n = 6$ injections into 3 mice ($^{***}p < 0.001$, $^{**}p < 0.01$).

sensitive agents against various external stresses commonly encountered in the respective applications.

2.6. Biocompatibility of HPODs

In contrast to natural polymers or small molecules, synthetic polymers are tunable, can tolerate a wide range of temperatures, are durable, and resistant to harsh conditions. Often their main limitation is a lack of biocompatibility, especially when used at high concentrations. Our findings indicate that higher concentrations of HPOD generally performed better in preserving biological activity across most tested applications. As the process of removing excipients prior to utilizing a biotherapeutic is tedious and not a sustainable practice in most applications, we performed a comprehensive evaluation of in vitro toxicity and in vivo tolerance of our HPOD library. We looked at cell viability, blood clotting, platelet activation, and RBC lysis for the different molecular weights and at high concentrations (see Figures S23 and S24, Supporting Information). Our testing revealed no influence on blood clotting using coagulation assays activated partial thromboplastin time (aPTT) and partial thromboplastin time (PTT), no hemolysis, and no platelet activation under all tested conditions. Incubation with endothelial and fibroblast cells did not lead to a decrease in cell viability for any of the tested conditions.

After seeing good hemocompatibility and in vitro tolerance, we evaluated the toxicity of HPOD in mice where a single escalating dose (up to 500 mg kg^{-1}) of HPOD was injected intravenously. The dose range selected based on the fact that the highest dose injected is ≈10 times lower than the maximum that will be injected in the case of a cryopreserved therapeutic. Blood samples and organs were assessed after 1 d and 14 d to test for acute and chronic toxicity and compared to saline injected controls (**Figure 6**). We examined the levels of alanine aminotransferase (ALT) and aspartate amino transferase (AST) to detect any indications of liver damage. Serum levels were not elevated compared to the saline control at either time point. In addition, no increase in lactate dehydrogenase (LDH) levels was found, suggesting no tissue damage. There are no significant changes in the body weights of the mice after the injection in comparison to saline control (Figure 6e). Finally, major organs were harvested 14 d after HPOD injection with the highest concentration and examined histologically. Tissue sections were stained using hematoxylin and eosin (H&E) and examined for tissue damage in a double-blind study (see Figure 6f). Pathological examination found no abnormalities in comparison to the control mice injected with saline. Taken together, these data prove that HPODs are well tolerated both in vitro and in vivo. This indicates that HPODs are ideal candidates to be used as excipients in the context of stabilizing biotherapeutics against heat, freezing, and lyophilization and may not have to be removed before administration.

2.7. The Influence of Architecture, Topology, and Hydration of HPODs

Having investigated the application of HPODs in the preservation of different types of biotherapeutics, we looked further into their structural features that provide high hydration and

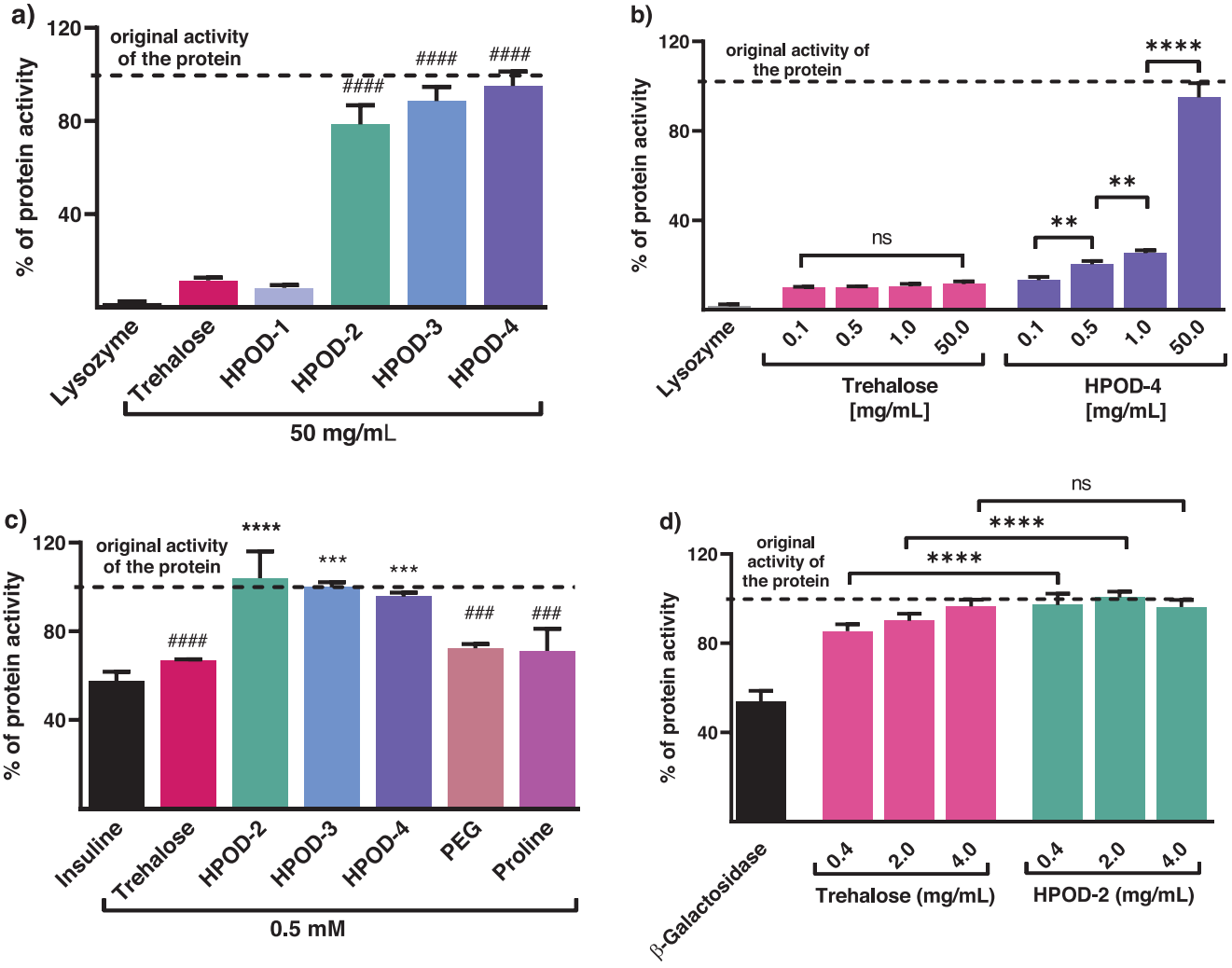

preservation properties. More specifically, we investigated the branching and branching-dependent hydration features of HPODs. We also investigated the hydration characteristics of hyperbranched polyglycerol (HPG) and polyglycerol dendrimer (PGD) generation 3, two representative polyether polyols with different branching characteristics.[32,35,39]

The hydration of HPOD polymers is clearly dependent on the molecular weight and branching of the polymers. The low molecular weight polymers have more bound water molecules compared to the high molecular weight HPODs (**Figure** 7a). The degree of branching and thus, the topology of HPOD, also influences the hydration properties (Figure 7b). A steep increase in the hydration is observed when the degree of branching decreases from ≈46% to 23%. Above and below this limit, the bound water molecules per monomer unit seem to be getting saturated. Particularly, the significant presence of linear units and the extended dendritic units (Figure S11, Supporting Information) in HPOD offer a more open branching structure and space to hold a higher number of water molecules compared to polymers with higher branching.

Based on the branching- and MW-dependent hydration properties of HPOD, we next investigated the hydration of those similar polyether-polyol families of dendritic polymers with different degrees of branching. We anticipated that this would provide additional evidence of the influence of polymer topology on hydration. We compared the hydration properties of HPOD (DB 40%), hyperbranched polyglycerol (HPG) (DB 57%),[35] and polyglycerol dendrimer (PGD)[39] (DB 100%) of similar molecular weight (Figure 7c). These polymers have a similar chemical composition but are topologically different due to the differences in branching structure (Figure 7c; Figure S11, Supporting Information). Since we are using similar molecular weight polymers, any change in the number of bound water molecules could only be attributed to the topological differences of the polymer. HPOD is found to have higher hydration (≈247 bound water molecules per polymer) compared to HPG (209 bound water molecules) and PGD with 140 bound water molecules (see Figure 7d; Figure S13b, Supporting Information). The number of water molecules associated with these polymers increases as the degree of branching (DB) decreases. We attribute this increase to the additional non-freezable water molecules accommodated in the space created by the linear extensions within HPOD compared to HPG or PGD, as well as the greater availability of hydroxyl groups within the polymers. The larger hydrodynamic size of HPOD supports the presence of additional space within the polymer structure.

HPOD exhibits ≈76% more bound water molecules than PGD of similar molecular weight; PGD has a more compact structure with hydroxyl groups located only on the outer periphery. Additionally, HPOD demonstrates higher hydration levels than the disaccharide trehalose, manifesting the outstanding hydration characteristic of HPOD (Figure S13b, Supporting Information; ≈44 water molecules/molecule of trehalose (378 amu) and 176 water molecules per polymer if the molecular weight is extrapolated to that of HPOD (1500 Da)).[59] The higher hydration of HPOD is further supported by its slower diffusion rate and larger hydrodynamic size compared to HPG or PGD (Figure 7d). Furthermore, MALDI-ToF spectra of HPG, HPOD-1, and HPOD-2 are presented in Figure S12 (Supporting Information) next to ESI spectrum of HPOD. The MALDI-TOF spectra of both HPODs reveal not only the expected mass peak distribution indicative of its repeating units but also the presence of adduct peaks. These adduct peaks correspond to the HPOD molecule complexed with water molecules (18 m/z), with multiplicities of 2, 3, or 4 water molecules observed, as detailed in Table S3 (Supporting Information). This finding is similar to that reported in the case of sugar molecules.[38] However, HPG[37] and PGD[39] do not show any water adducts. The MALDI-ToF data supports the unique hydration behavior of HPOD, which is unlike other polyether polyols of similar chemical composition. Together these data support our claim that the structure and topology of these polymers are influencing the hydration characteristics even though these polymers have similar molecular weights, number of hydroxyl groups, and a polyether polyol backbone.

In an attempt to correlate the hydration features to the cryoprotection ability of HPODs, we looked at their ice recrystallization inhibition efficiency in comparison to hydroxyethyl starch (HES) and polyvinyl alcohol (PVA).[60,61] Ice recrystallization refers to the growth of large crystals at the expense of small crystals, a process that can disrupt cells, protein structures, or soft particles like LNP during a freeze-thaw cycle. The ice recrystallization inhibition efficiency of these agents was determined by rapidly freezing sucrose-water solutions containing different polymers (HPOD,

Figure 5. Stabilization of proteins against heat, lyophilization, and freezing. a) Activity of lysozyme after heating (60 °C, 30 min) in the presence of different HPODs and trehalose at 50 mg/mL. Lysozyme refers to the protein activity after heating without any excipients. HPOD-**2**, **3**, and **4** showed enhanced activity compared to trehalose ($n = 3$, $^{\#\#\#\#}p < 0.0001$. b) Screening of concentration range for trehalose and HPOD-**4** for protection against heat shock at 60 °C of lysozyme. HPOD-**4** showed concentration dependent activity whereas trehalose did not show any improved activity with concentration. c) Preservation ability of HPODs against insulin aggregation upon heating (60 °C, 48 h) in comparison to different additives ($n = 3$). The activity of the original insulin is also demonstrated, specifically referring to the absence of fibril formation. HPODs showed high efficiency in protecting insulin and is superior to the most commonly studied macro and small molecular additives, including trehalose, proline, and PEG (HPOD-**2** versus trehalose ($^{\#\#\#\#}p < 0.0001$), versus proline ($^{\#\#\#}p = 0.0003$), and versus PEG ($^{\#\#\#}p = 0.0005$)). All HPODs showed enhanced activity compared to trehalose (trehalose versus HPOD-**2** ($^{****}p < 0.0001$), versus HPOD-**3** ($^{***}p = 0.0003$), and versus HPOD-**4** ($^{***}p = 0.0009$). d) Protection of β-galactosidase from lyophilization stress using HPODs ($n = 12$). HPOD-**2** and trehalose protected β-galactosidase even at very low concentrations (0.4 mg mL^{-1}). HPOD-**2** showed improved performance at low concentrations compared to trehalose, however, there was no significant difference found at higher concentrations (trehalose versus HPOD-**2** (0.4 mg mL^{-1}, $^{\#\#\#\#}p < 0.0001$), (2 mg mL^{-1}, $^{\#\#\#\#}p < 0.0001$), and (4 mg mL^{-1}, ns). **e**) Preservation of function of anti-blood group A antibody after freezing for 3 freeze-thaw cycles, where each cycle is performed within 24 h. The antibody activity after each freeze-thaw cycle is shown and the dotted line represents the activity of fresh antibodies that did not undergo freezing and the bars represent the activity of stored antibodies mixed with the presented excipients. Trehalose is a known excipient and used as a comparison for our HPOD excipients (N = 6 from 3 blood donors). Both HPOD-**2** and HPOD-**4** preserved antibody function after three repeated freeze-thaw cycles (one cycle every 24 h), and it is more efficient than trehalose (trehalose versus HPOD-**4** ($^{\#\#}p = 0.0030$ (Day 1), $^{\#\#}p = 0.00545$ (Day-2), and n.s. (Day 3)); trehalose versus HPOD-**2** ($^{\#\#\#}p = 0.0005$ (Day 1), $^{\#\#}p = 0.0029$ (Day-2), and n.s. (Day 3)). Fresh antibody aliquot that never went through freeze-thaw cycles was used as a control. All the data were reported as mean ± s.d.

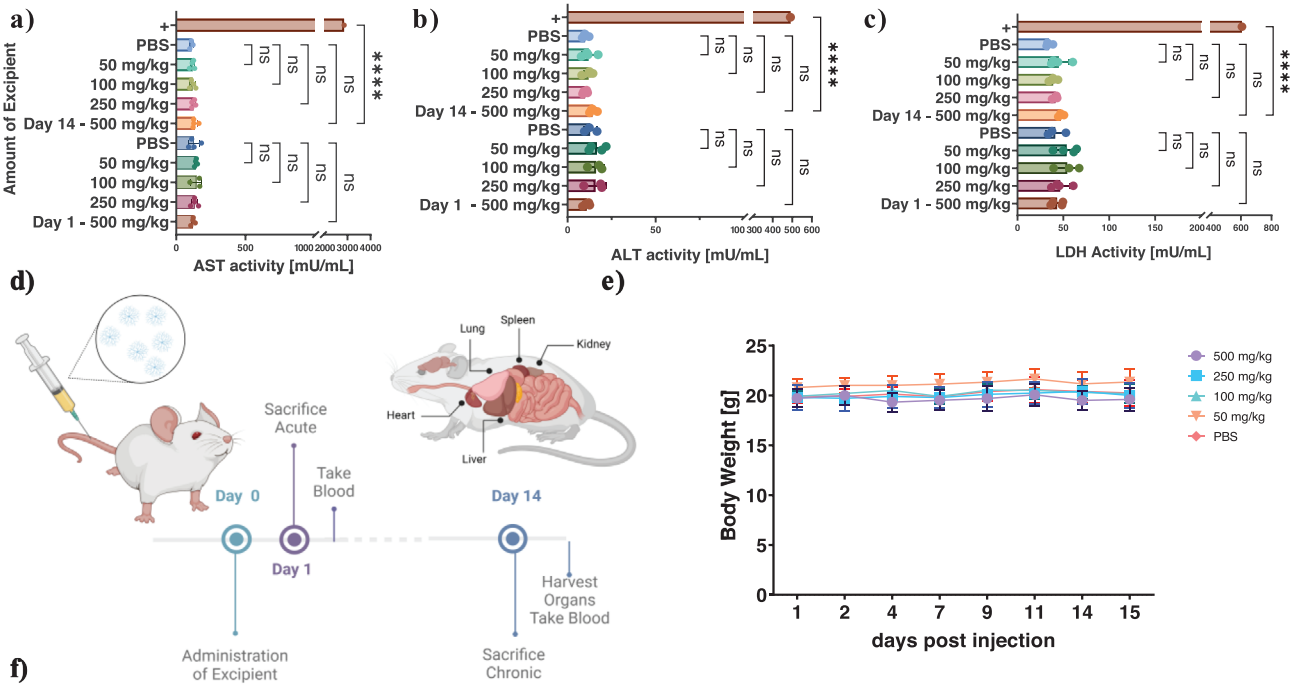

Figure 6. Tolerance of HPOD in mice. a–c) There is no significant increase in AST, ALT, and LDH levels compared to PBS (1x, pH 7.4) control as determined from mice sera taken on day 1 and day 14 after i.v. injection of HPOD at concentrations between 50 and 500 mg kg^{-1}. That indicates that HPOD was well tolerated in mice at high doses. d) Schematic representation of the injection model. BALB/c mice were administered the excipient at a dose of up to 500 mg kg^{-1} of HPOD. The mice were monitored daily and body weights were observed. After 1 and 14 days, serum and organs were collected from sacrificed mice and analyzed. The figure was created using BioRender.com. e) There was no change in body weight observed for mice injected with the excipient compared to mice injected with saline. f) Representative images of stained (H&E) organ slices collected from mice injected (i.v.) with 500 mg k^{-1}g HPOD and PBS (1x, pH 7.4). No abnormalities were seen in the heart, lungs, liver, and kidneys of mice. All the data were reported with as mean ± s.d. of n = 4 mice per group.

PVA, and HES) at ≈−50 °C to form small ice crystals (≈15 µm radii), and then annealing the samples at ≈−9 °C and monitoring the growth of large ice crystals (measurements of the diameter of the crystals in Figure 7f) at the expense of small ice crystals during the annealing process using cryomicroscopy (Figure 7e). While the concentration of HPOD-4 showed a significant influence on the growth of large ice crystals (see Figure S14, Supporting Information), the recrystallization inhibition was not different from sucrose and HES, indicated by non-significant differences in ice crystal diameters (see Figure 7f).[61,62] Based on the current data, HPOD and HES in sucrose solution exhibited less ice recrystallization inhibition compared to PVA. However, these substances demonstrated their effectiveness in cryopreservation, suggesting the presence of an alternative mechanism, possibly involving the formation of a hydrated matrix around LNPs or proteins.[62]

3. Discussion

Preserving the activity of biotherapeutics is a crucial aspect of their development, as it greatly influences their pharmaceutical applicability. The importance of cryoprotective excipients became evident through their utilization in the approved mRNA-vaccines Comirnaty (BioNTech/Pfizer) and Spikevax (Moderna) during

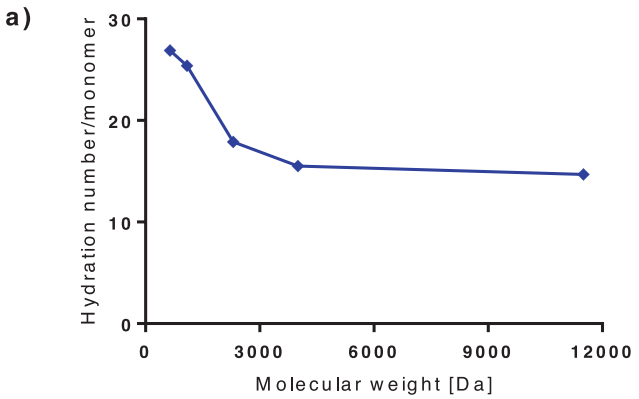

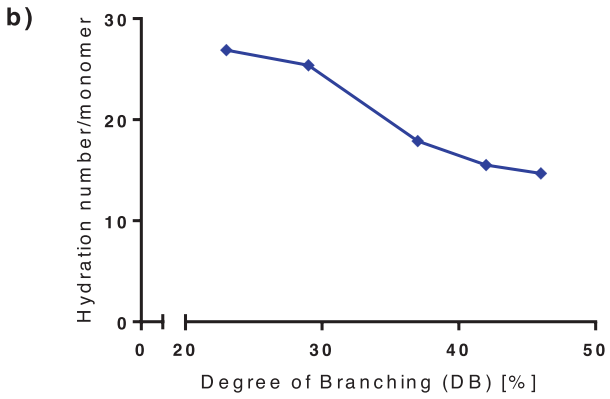

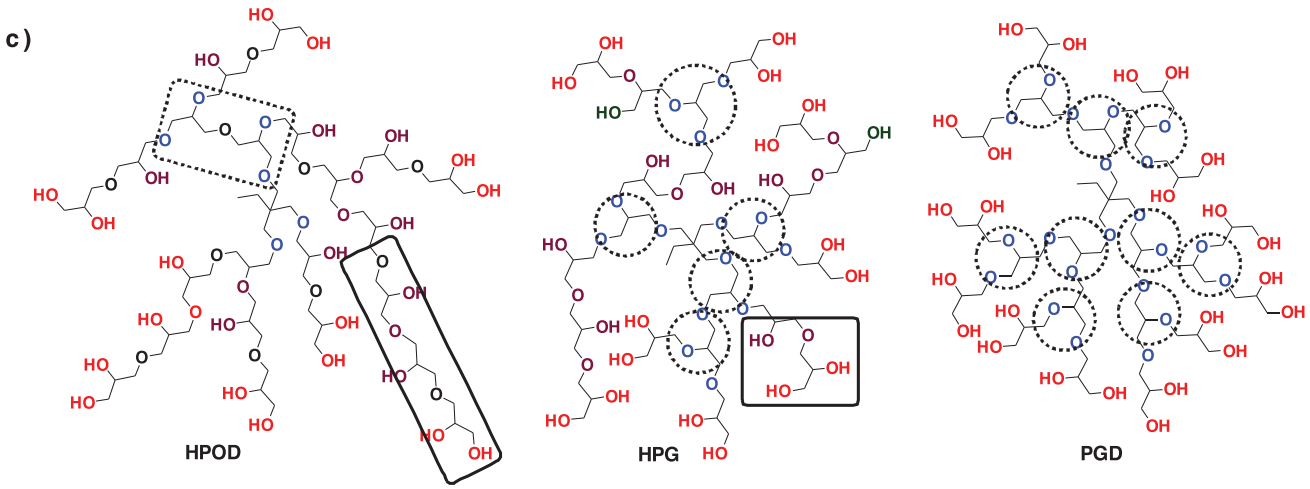

d)

Polymer	M_n [Da]	DB [%]	Diffusion coefficient (D)*10^{11} [m^2/s]	Hydrodynamic size [nm]	Hydration number /molecule
HPOD	1450 (1.1)	40	9 ± 0.40	3.8 ± 0.16	247 ± 6.0
HPG	1500 (1.1)	57	18 ± 0.05	2.4 ± 0.06	209 ± 7.6
PGD	1696 (1.0)	100	20 ± 0.03	2.2 ± 0.02	140 ± 2.1

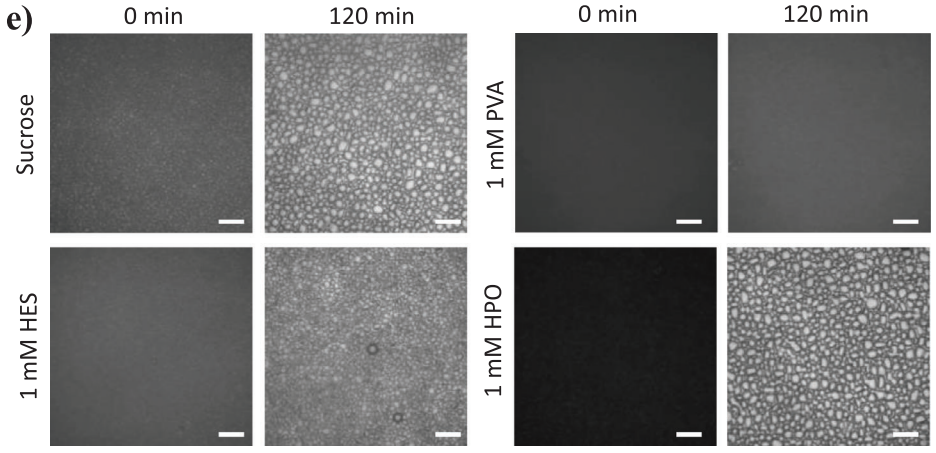

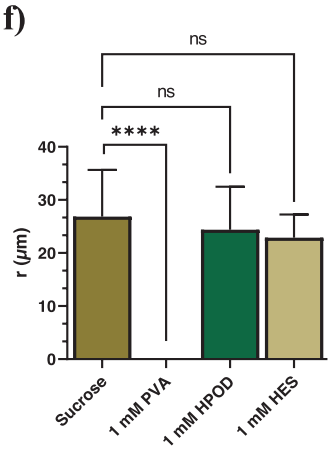

the COVID-19 pandemic.[54,63] Given the anticipated growth of research in the field of LNP technology, it is important to address compatibility challenges and enhance stabilization methods to fully realize their potential. Exploring the avenue of lyophilization offers a promising opportunity for further investigation and advancement. Developing excipients for LNP protection poses several challenges due to the complex nature of the particles and their predisposition to various degradation pathways, such as the denaturation of the cargo, particle aggregation, or bursting. Excipients need to stabilize the RNA-LNPs and prevent or minimize these degradation processes during storage and administration, while at the same not interacting adversely with the RNA-LNPs in a way that would lead to structural changes or decreased activity.[63] Compatibility issues can arise due to pH, ionic strength, or specific interactions between excipients and particles.[64] Ideal excipients allow for formulation flexibility, including various dosage forms such as liquid solutions or lyophilized powders.

Similar challenges are faced in the development of excipients for proteins because of their susceptibility to denaturation, aggregation, oxidation, and proteolysis.[1,2,11,65,20,66–68] There is a high demand for improved cryoprotectants, where hemotoxicity, immunogenicity, cytotoxicity, synthetic challenges, and difficulty in the generation of pharmaceutical grade compounds prevent the advancements in this field.[1] Approved excipients include sucrose in antibody formulations (e.g., KEYTRUDA (pembrolizumab)), PEG, and sorbitol are used in Ogivri, and human serum albumin is used in Blincyto.[66] Further, trehalose is used as an excipient in many commercially available therapeutic products, including Herceptin, Avastin, Lucentis, and Advate.[65] Those excipients used, however, are not applicable to diverse pharmaceutical products and each application necessitates the evaluation and identification of suitable excipients.[69]

Here, we show the development of a new class of highly biocompatible branched polymer, (hyperbranched poly(3-(oxiran-2-ylmethoxy)propane-1,2-diol) (HPOD)), with exceptional hydration properties and showcase their excellent excipient properties. HPODs exhibited a unique capability to effectively preserve both mRNA- and saRNA-LNPs, stabilize them against degradation (see Figures 3 and 4), and protect a spectrum of protein therapeutics (see Figure 5), safeguarding them against various stressors such as freeze-thaw cycles, lyophilization, and heat. Even though there was no consistent molecular weight to function relationship, HPODs as one class of polymer did preserve a variety of pharmaceutical products by generating a topologically diverse polymer library that competed with or outperformed currently available agents including GRAS excipients in terms of stabilization and cryoprotection abilities. Our investigation prioritized freeze-thaw cycles over long-term studies because we focused on the stabilization throughout these structurally more severe events. Additionally, we aimed to have a well-defined baseline for each experiment, which was only possible with using the freshly prepared RNA-LNPs as the internal reference. As we transition into the post-pandemic era, robust data on long term preservation will become paramount for optimizing future endeavors.

For now, in the design of HPOD polymers, we have considered several factors. There are no established design criteria reported for the development of macromolecular stabilizing agents. As a general principle, most of them have one of the key features, such as high polarity, charge, hydrophilicity, being zwitterionic, or distinct hydrophobic pockets in their molecular architecture.[70] In the context of cryopreservation, it was found beneficial to have a sheath of non-frozen bound water present in the molecule.[71,72] Thus, we have synthesized a new polymer which has large number of hydroxyl groups in a branched polyether backbone. The low intrinsic viscosity, compact nature, and high biocompatibility shown by HPOD is due to its branched structure and is consistent with reports of branched polymer structures offering notable advantages over linear structures.[32] More criteria we took into account were the high water solubility and the potential ability to bind unfreezable water molecules. We believe that our polymer has sugar-like hydration (see the MALDI data) and behavior at lower molecular weights; and it functions similarly to other hydrophilic macromolecules at higher molecular weights used for cryopreservation. This is most likely the reason that we have good preservation for this wide variety of biotherapeutics at a range of physical stressors. In the case of heat protection, we hypothesize that the polymers form a hydration shell around the biomolecules, which could help to maintain their native structure by stabilizing hydrogen bonds and preventing denaturation due to heat. Additionally, the increased viscosity compared to aqueous buffer reduces the molecular motion and thus decreases heat stress. The highly hydrated polyether structure of HPOD, is shown to impart this property. Additionally, the polyol structure of HPOD serves the purpose of mimicking sugar molecules, which are known to have preservation properties.[67] The utilization of a sugar-mimicking polymers such as HPOD over sugars provides notable advantages, such as lower osmolarity and enhanced stability while allowing for fine tuning of the preservation capability, particularly when higher concentrations of cryoprotectant are needed. However, additional long-term studies are needed to fully realize the potential of this new excipient.

Figure 7. Comparison of hydration of HPODs with polyglycerol polymers. Influence of a) molecular weight and b) degree of branching (DB) on the hydration of HPODs. With increase in molecular weight and DB, hydration of the HPODs is significantly decreased and reaches saturation rapidly when the molecular weight is >4000 Da as well as when DB is ≈40%. c) Schematic representation of chemical structures of three macromolecules; HPOD, hyperbranched polyglycerol (HPG), and polyglycerol dendrimer (PGD) with varying degrees of branching 40, 57, and 100% respectively. The number of dendritic units (dashed circles) and the nature of liner units (solid squares) of HPOD are quite different from HPG. d) Hydration of the macromolecules is influenced by DB. HPOD was found with more bound water molecules than HPG or PGD, demonstrating the influence of polymer topology. The hydrodynamic size ($2R_h$) of the HPOD was measured by the Stokes-Einstein equation, $R_h = kBT/6\pi\eta Dt$; Dt was determined using pulse-field gradient nuclear magnetic spectroscopy. **e)** Cryomicroscopic images of ice crystals formed in the presence of polymers after annealing at −9.1 °C. The samples (1 mM solutions of HPOD-4, PVA (8 kDa), and HES (180 kDa) in 30% sucrose and sucrose without any additives) were cooled to −50 °C to form small ice crystals (≈15 µm radii) and then annealed at −9.1 °C while recording images of the ice crystals during annealing (scale bar – 100 µm). A representative set of images recorded after annealing at −9.1 °C for 0 and 120 min are shown here. f) Size of crystals represented here as average radii of 45 crystals. This study shows that HPOD works in a similar matter to HES but differs from PVA in its influence on ice recrystallization inhibition.

Our studies also identified a key feature — polymer topology— , which has not previously been explored in the development and production of cryo- and lyo-protecting macromolecular excipients. Our findings demonstrated that the introduction of linear units within the branched structure had a remarkable effect on the amount of bound water molecules associated with HPOD (Figure 7) compared to similar polyether and polyol building blocks such as HPG and PGD (chemically identical but with a difference in topology). Further, we found a sharp increase in the amount of bound water molecules with a decreasing degree of branching until ≈42% (Figure 7b). We believe that a low branching density and the resulting flexibility allowed for the formation of an optimal water structure within and around HPOD. The chain confinement presents in PGD (100% branching) resulted in a significant drop in the bound water (76% decrease; Figure 7c,d) possibly due to steric factors as the dendrimer interior cannot accommodate such large amount of water molecules even though the theoretical possibility of hydrogen bonding with water exists. A synergy of all these effects resulted in the exceptional hydration of HPOD, which was as high as 27 bound water molecules per monomer unit, higher than any known molecule. We believe that structural features, such as linear units within branched structures which provide increased space for water molecule binding, chain confinement due to branching, and the polyether-polyol structure that facilitates extensive hydrogen bonding are all contributing toward the generation of a stable non-freezing bound water layer around and within the HPOD resulting in high hydration. The hydrated molecular ions seen in MALDI-ToF spectra of HPOD are further demonstrating that the water molecules are very tightly bound to HPOD. Such water adducts are rarely seen with polymer ions, they are more common for sugars.[38]

Based on our findings, while HPOD exhibited similar performance to sucrose and HES, it did not match the efficacy of PVA in inhibiting ice recrystallization (Figure 7e,f). Therefore, the inhibition of ice recrystallization alone does not provide a conclusive explanation for the performance of HPOD in preserving proteins and RNA-LNPs at very low temperatures. As ice recrystallization inhibition has been identified as an important process in the protection of sensitive material during a freeze-thaw cycle,[21,30,70] other mechanisms must be acting together to generate the preservation properties of HPOD. The generally accepted mechanisms with respect to macromolecular excipients in the context of protecting proteins and biotherapeutics from different external stresses are vitrification, preferential exclusion, and water replacement. All of these are associated with the alteration of the water structure around the proteins to preserve their native conformation and might be acting in the case of HPOD. With its extended hydration sphere, HPOD may form strong interactions with proteins and LNP components, providing a response to the external stimuli and thereby preserving the integrity of the stored cargo.

HPOD effectively solved many preservation challenges with a single polymer class. It also exhibits remarkable biocompatibility. We anticipate that this would simplify the formulation process, reduce complexity, and potentially improve the stability and functionality of future LNP- and protein-based therapeutics for clinical applications. Although HPOD has remarkable properties, further immunogenicity studies, long term preservation studies, upscaling of the synthesis, and possibly improvement in the synthesis process are needed to further validate these new macromolecular excipients for future clinical use.

4. Experimental Section

Synthesis: All reagents, solvents, and molecular sieves (4 Å) were purchased from Sigma–Aldrich, Canada, unless otherwise mentioned. Deuterated solvents (D_2O and MeOD 99.8% D) were purchased from Cambridge Isotope Laboratories, Inc. Standard regenerated cellulose (RC) membranes (MWCO-0.5, 1, 3.5, and 5 kDa) for dialysis were purchased from Spectrum, Inc., USA. NMR spectra (^1H, ^{13}C, ^{13}C inverse-gated (IG), HSQC, DEPT-135, and diffusion coefficient measurements (D)) of polymers were recorded on Bruker Avance 300 and 400 MHz spectrometers. The degree of branching (DB) of the polymers was calculated using the equation, DB = 2D+sD/(2D+(4/3)sD+2/3L), where D, sD, and L represent the intensities of the signals corresponding to the dendritic, semidendritic and linear units respectively, which were determined using ^{13}C IG NMR spectroscopy (D_2O, relaxation delay of 6 s).[36,73,74] The determination of the DB was based on approximation and theoretical probability of the formation of structural units in AB3. Since identifying the actual structural linkages in HPOD using AB3 kinetics were a significant project on its own, the peaks using AB2 calculations (L13, D, 2L14, 2D, 2T, L13, L14, T, L13) were initially labeled. These labeled peaks were then utilized to assess the probability of peaks forming according to AB3 calculations as shown in Figure S11 (Supporting Information). These units were further categorized as D+T, L13+14, 2L14, D+L13, D+L14, 2D, L14+T, linkages. By considering the similar chemical nature of these linkages with AB2 structural linkages and the theoretical probability of formation of structural units in AB3 (T:L:SD:D at a probability of 8:12:6:1), the probability of formation for the remaining linkages (D, T, L13, and L14 linkages are determined. For specific calculations see the provided supplementary file. The absolute molecular weight of the HPODs was determined by a Water size exclusion chromatography system fitted with multi angle laser light scattering (MALS) detector (DAWN HELEOS II) and refractive index detector (Optilab T-rEX). Viscometer (Viscostar II) detector was used to measure the intrinsic viscosity of the polymers in a 0.1 N $NaNO_3$ buffer (pH 7.0) mobile phase. All the detectors were from Wyatt Technologies, Inc., Santa Barbara, CA. Gel permeation chromatography analysis was performed using Waters ultrahydrogel columns (guard, linear, and 120) and 0.1 N $NaNO_3$ buffer (pH 7.0) was used as a mobile phase, and dn/dc value for HPODs was determined as 0.12 mL g^{-1}. Fusion enthalpy of polymer solutions and water was determined using differential scanning calorimetry (DSC) (Q2100, TA instruments, New Castle, DE, USA). All the DSC data was processed using TA instruments universal 2100 software. Thermite pans and lids were purchased from Perkin Elmer. Absorbance measurements were performed on SpectraMax M3 (Molecular Devices). Fluorescence measurements were carried out on a Cary Eclipse fluorescence spectrophotometer (Agilent). Confocal imaging was carried out on a Nikon C2+Confocal Microscope System. Polyglycerol dendrimer (PGD) (generation 3) was synthesized and characterized by following a previous report.[75]

Synthesis of 3-(oxiran-2-ylmethoxy)propane-1,2-diol (OPD) Monomer: *m*-Chloroperbenzoic acid (*m*-CPBA) (37.6 G, 0.168 mol, 1.5 eq, 77 wt%) was added in small portions to a solution of 3-allyloxy-1,2 propanediol (15 G, 0.112 mol) in DCM (250 mL) at RT and the reaction mixture was stirred for 20 h. A white precipitate, *m*-chlorobenzoic acid as a by-product, was noticed over time in the flask and the reaction mixture was filtered to remove the *m*-chlorobenzoic acid. The volume of the filtrate was slightly concentrated (≈25–30% of the original volume or until a small amount of precipitate was noticed in the flask) and the flask was kept at 0 °C to further precipitate and filter out the *m*-chlorobenzoic acid. The concentration-precipitation-filtration cycles were repeated for three more times and the final 100–120 mL of DCM solution was washed with 100 mL of water three times. The water fraction also contained a small amount of m-chlorobenzoic acid, which was confirmed by ^{1}HNMR. To remove it, the collected 300 mL of aqueous fraction was washed three times

with 100 mL of EtOAc. The obtained water layer was lyophilized until the water content (analyzed by thermogravimetry analysis) in the monomer was ≈1% (yield: 60–70%). The structure of the monomer was determined by NMR (Figures S2–S4, Supporting Information) and mass spectroscopy. ^{1}H NMR (400 MHz, D_2O-d_2): δ 2.78 (m, 1H), 2.96 (t, J = 4.44 Hz, 1H), 3.37 (m, 2H), 3.60 (m, 4H), 3.91 (m, 2H). ^{13}C NMR (75 MHz, D_2O-d_2) 45.01, 51.75, 62.64, 70.50, 72.07, 72.15. HRMS (TOF ES+): Calcd for $C_6H_{12}O_4$: 148.07 [m/z],171.07 [m+Na].

Synthesis of Hyperbranched poly (3-(oxiran-2-ylmethoxy) Propane-1,2-diol (HPOD) Polymers: HPOD polymers were synthesized using anionic ring opening multibranching polymerization.[73,74] A representative synthetic procedure for HPOD-**3** was described in the following section. Briefly, trimethylolpropane (82 mg, 0.61 mmol) was taken in a flame dried three neck flask and KOMe (74 µL, in 25% MeOH) was added under argon, stirred for 30 min at RT. After methanol was evaporated at 70 °C for 4 h, reaction temperature was raised to 90 °C. The flask was connected to an overhead stirrer and OPD monomer (3.1 g, 21 mmol) was added slowly (0.25 mL h^{-1}) under argon using a syringe pump After the addition was completed, the reaction mixture was stirred for an additional 5 h. The reaction mixture was quenched with a very small amount of 0.01 M HCl to reach a neutral pH. The polymer was precipitated twice by dissolving in MeOH and precipitating with an excess amount of from MeOH/diethyl ether (1:9 v/v). The precipitated polymer was purified by dialysis against cellulose membrane (MWCO-0.5 kDa) for 24 h (dialysate replacements for every 4–5 h) (yield 40%). The molecular weight and structural characterization of the polymers were performed by gel permeation chromatography and NMR spectroscopy respectively. The purified polymer has a molecular weight of 2300 (M_n) and polydispersity (M_w/M_n) (1.2) was determined from gel permeation chromatography analysis. The dn/dc of HPOD polymer was 0.12 mL g^{-1}. The NMR structural analysis was given in Figures S5,S6, and S11, and Table S4 (Supporting Information). The monomer to initiator ratios and other conditions used for the synthesis of the rest of the HPODs are given in Table S1 (Supporting Information). For HPOD-**1**, simple precipitation protocols (MeOH/diethyl ether) were used to get the desired polydispersity of the polymer and dialyzed for a short period of time to remove any organic solvents (MWCO-0.5 kDa, 8 h). For HPOD-**2** and **3,** after precipitation, dialysis purification was sufficient enough (MWCO-0.5 kDa) to get the polymers with desired molecular weight. For HPOD-**4**, after precipitation, either the dialysis or the fractional precipitation purification method was employed depending on the amount of lower molecular weight fractions in the crude reaction mixture. For HPOD-**5**, after precipitation, the fractional precipitation method was adopted by maintaining the constant volumes of methanol and varying the volumes of diethyl ether and finally dialyzed (MWCO-3 kDa) to remove any organic impurities. ^{1}H NMR (400 MHz, D_2O-d_2): δ 0.83 (m, 3H), 1.29 (m, 12), 3.37 (m, 2H), 3.40-4.20 (m, 10H). ^{13}C NMR (75 MHz, D_2O-d_2): 61.0, 62.5, 69.0, 69.4, 71.6, 71.8, 72.4, 78.0, 79.6.

Hydration Studies of HPODs: Hydration of the HPODs was determined using differential scanning calorimetry (DSC). All the samples were dried at 40 °C under vacuum for overnight and make sure that the water content was very minimal by TGA. The dried polymer was used to prepare the polymer solution (7–10% W/W) in Milli-Q purified water, and ≈20 µL was loaded into a Tzero aluminum hermetic sample pan and closed with an appropriate lid. The sample pan was cooled down to −20 °C and warmed to −5 °C at the rate of 2 °C min^{-1}. Heating of the sample was further continued from −5 °C to +5 °C at the rate of 0.2 °C min^{-1} and to +20 °C at the rate of 2 °C min^{-1}. The enthalpy of fusion of polymer solution or pure water was determined by integrating the area under the respective peak of DSC trace. An empty pan was used as a reference. The same protocol was repeated for all HPODs, hyperbranched polyglycerol (HPG), polyglycerol dendrimer (PGD), and trehalose.

The number of water molecules bound per polymer was calculated using the following equation.

$$[N_{bw}] = \left[\Delta H_{fo}\left(Wt_w - Wt_p\right) - \Delta H_{fps} \times Wt_{ps}\right] / \left[\Delta H_{fo} \times MW_{H2O} \times Np\right] \quad (1)$$

N_{bw} = number of water molecules bound per polymer

ΔH_{fps}, ΔH_{fo} = fusion enthalpy of polymer solution and pure water respectively

Wt_w, Wt_p, Wt_{ps} = weight of the pure water, pure polymer alone, and polymer solution respectively

Np = number of moles of polymer taken.

Since HPODs were highly hydrated, the correction factor for moisture content was applied to obtain the actual weight of the polymer based on the thermogravimetric analysis data. Each of the hydration measurements were repeated at least twice.

Hydrodynamic Size and Diffusion Coefficient Measurements: Diffusion coefficient of different polymers was determined by pulse field gradient-nuclear magnetic resonance (PFG-NMR) experiments using 400 MHZ spectrometer at 25 °C, using D_2O as a solvent.[76–78] The parameters (T1-spin/lattice relaxation, P_1-90° pulse, δ-the width of a bipolar pair, and Δ-the diffusion time) of the experiment were optimized, and the data was acquired using a pulse program, Ledbpgp2s (from Bruker). The gradient strength (G) was altered from 1 to 32 G/cm in 16 steps (Figure S8, Supporting Information). Free induction decays were averaged over 8 scans using 4 dummy scans. The diffusion coefficient (Dt) was extracted (XWINNMR-3 software) using a non-linear square curve fitting to the relationship between pulse field gradient and echo attenuation, by the following equation.

$$\ln[A/Ao] = -Dt\left[\gamma^2 G^2 \delta^2 (\Delta - \delta/3)\right] \quad (2)$$

Hydrodynamic radius (R_h) was determined by Stoke–Einstein equation ($Dt = kBT/6\pi\eta R_h$) using the diffusion coefficient obtained from PFG-NMR experiments.

Mass Spectrometry Characterization of HPG and HPOD: HPG and HPOD samples were characterized, following purification, using Matrix-Assisted Laser Desorption/Ionization-Time of Flight (MALDI-TOF) and Electrospray Ionization (ESI) mass spectrometry to determine the molecular weight of the sample and the repeating units. The samples were dissolved in Milli-Q water at 1 and 2.7 mg mL^{-1} for MALDI-TOF and ESI, respectively. To prepare the matrix for MALDI-TOF mass spectrometry measurements, 2,5-dihydroxybenzoic acid (DHB) was dissolved in 50:50 acetonitrile: water solution at 10 mg mL^{-1}. Ten microliter of the matrix was mixed with 1 µL of the sample and 1 µL of the sample/matrix mixture was deposited onto the MALDI target plate. The measurements were obtained on a Bruker Autoflex Speed LRF MALDI-TOF in positive ion linear mode. Prior to ESI mass spectrometry measurements, the sample was analyzed by a Hewlett Packard 1100 series High-performance liquid chromatography (HPLC) system using 100% acetonitrile as the mobile phase. Following HPLC, ESI mass spectrometry measurements were obtained on a Bruker HCT Ultra PTM in positive mode.

LNP Cryopreservation Studies—Materials: CleanCap EGFP mRNA (5moU) was purchased from Cedarlane, mRNA encoding for firefly luciferase (fLuc) and saRNA (fLuc) were synthesized using MEGAscript T7 transcription kit from Invitrogen and was capped using the ScriptCap Cap1 capping system purchased from CELLSCRIPT, Cholesterol, 18:0 PC (DSPC) 1,2-distearoyl-sn-glycero-3-phosphocholine, powder, and DMG-PEG2K were obtained from Sigma–Aldrich, DLin-MC3-DMA was obtained from NanosoftPolymers (Salem, USA), NanoAssemblr Ignite Cartridges were purchased from Precision Nanosystem, Rediject D-Luciferin Bioluminescent Substrate was purchased from PerkinElmer (USA).

LNP Cryopreservation Studies—LNP Preparation and Preservation: mRNA-LNPs encoding for enhanced green fluorescent protein (EGFP) were prepared on a NanoAssemblr (Precision NanoSystems Inc., Vancouver, BC, Canada) at a total volume of 1.5 mL with a N/P ratio of 3:1 and a 12 mL min^{-1} flow rate. The aqueous mRNA-containing buffer solution (pH 4) is rapidly mixed with the lipids (proprietary to Acuitas, MC3/DSPC/Cholesterol/ PEG-Lipid 2000 at a ratio of 50/10/38.5/1.5) in ethanol and then diluted into phosphate buffered saline (PBS) and purified with Amicon 10k MWCO. Typically, the mRNA-LNP solutions were used at concentrations between 120–200 µg mL^{-1} for the preservation studies. Similarly, mRNA-LNPs and saRNA-LNPs encoding fLuc were prepared using the Pump 33 DDS Syringe Pump (Harvard Apparatus). The aqueous

phase (mRNA (fLuc) or saRNA (fLuc) in 25 mM sodium acetate buffer at pH 4.53) and lipid phase (consisting of SM-102/DOPE/Cholesterol/DMG-PEG-2000 at a molar ratio of 45:17.5:36.25:1.25 in ethanol) were rapidly mixed) with a N/P ratio of 10 and 16 mL min^{-1} flow rate. The prepared LNPs were then diluted into PBS and purified with Amicon filters (10K MWCO) to a concentration ≈150–200 μg mL^{-1}. The size and PDI were determined by dynamic light scattering (1:100 dilution in PBS) using a Zetasizer Nano ZS (Malvern Instruments Ltd., Malvern, UK), and the encapsulation efficiency (EE%) was determined using Quant-iT RiboGreen RNA Reagent and Kit (ThermoFisher) according to the manufactures protocol. To assess the integrity of encapsulated RNA, LNPs were subjected to lysis for RNA extraction, following established procedures.[79] In brief, LNPs were combined with an equal volume of 2% Triton X lysis buffer and incubated on ice for 10 min to facilitate LNP lysis. Subsequently, RNA was isolated using the Monarch 10 μg RNA Cleanup Kit (New England Biolabs), adhering to the manufacturer's recommendations. The eluted RNA was suspended in RNase-free water, and its concentration was adjusted to ≈≈250 ng μL^{-1}. RNA integrity was evaluated utilizing the Bioanalyzer RNA 6000 Nano Kit (Agilent Technologies), the 2100 Bioanalyzer Instrument (Agilent Technologies), and the Bioanalyzer 2100 Expert software (Agilent Technologies), following the manufacturer's protocol. The assessment involved calculating RNA integrity based on the total peak area and the fill transcript peak, as previously described.[80–82]

In order to be considered freshly prepared as a positive control for the preservation experiments, the LNPs were used as soon as possible but always within a week after preparation. For preservation experiments, the mRNA-LNPs and saRNA-LNPs were mixed at a volume ratio of 1:1 with cryopreserving solution prepared in Tris buffer (Tris(hydroxymethyl)aminomethan-HCl buffered solution, 20 mM, pH 7) at a final concentration of 20w/v of excipient, unless stated otherwise. Tris buffer only (20 mM, pH 7) was included as an unpreserved reference that goes through a freeze-thaw-cycle or lyophilization process as well. Preserved and unpreserved tubes were stored at 70 °C in a Mr. Frosty or lyophilized overnight. After thawing or reconstitution with MQ water, respectively, the LNPs were characterized by size, PDI, RNA integrity, and EE% measurement, and then used for cell transfection of CHO and HeLa cells. Results are compared to the freshly prepared batch stored in the fridge that has never been frozen or lyophilized.

LNP Cryopreservation Studies—Cell Culture: HeLa and CHO cells were cultured in EMEM and RPMI, respectively, supplemented with 10% heat inactivated fetal bovine serum (FBS) and 1% penicillin-streptomycin at 37 °C with 5% CO_2. For EGFP protein expression, cells were seeded at 50 000 cells per well in 48-well plates, cultured for 1d, and treated with 0.25 μg per well of mRNA. After 24 h of expression cells were dissociated with cell dissociation buffer, washed, and subjected to analysis by flow cytometry (CytoFLEX, Beckman Coulter). See Figure S19 (Supporting Information) for the gating strategy.

LNP Cryopreservation Studies—mRNA-LNPs and saRNA-LNPs Expression in BALB/c Mice: All animals were handled in accordance with the animal protocol (A21-0062) approved by the animal care committee, University of British Columbia. Female BALB/c mice aged 6–9 weeks were purchased from Jackson Laboratory (USA) and housed 3 per cage in fully acclimatized room with constant access to sterile food and water ad libitum. Mice were imaged as previously described.[82] Briefly, mice were intramuscularly injected (both hind legs) with 5ug of mRNA (fLuc) LNPs (with or without excipients) or 1ug of saRNA (fLuc) LNPs (with or without excipients) in a total volume of 50 uL. On the day of imaging, mice were intraperitonially injected with 150 uL Rediject D-Luciferin Bioluminescent Substrate. 7 min post injecting with the substrate, the mice were subjected to anesthesia (3-4% isoflurane) and imaged using the IVIS Spectrum In Vivo Imaging System (PerkinElmer) for 3 min. Living Image analysis software by PerkinElmer was used to quantify the signal from the site of injection.

Protein Stabilization Studies—Lysozyme Stabilization Assay: The lysozyme (Sigma–Aldrich) and Micrococcus luteus (Sigma–Aldrich) labeled with FITC were prepared at 100 U mL^{-1} and 1 mg mL^{-1} in water, respectively. The stabilizing agents, trehalose (Sigma–Aldrich), HPODs, and other polymers (PEG, HPG, dextran, and PDMA) were prepared in reaction buffer (0.1 mg mL^{-1}, DPBS, pH 7.4) at 50 mg mL^{-1} (final concentration). Lysozyme solution (50 μL) was mixed with 50 μL of stabilizing agent in a 1.5 mL Eppendorf and heated at 60 °C for 30 min in a water bath or lysozyme alone with buffer, then cooled in an ice-bath for 15 min. The intact lysozyme activity was measured with EnzChek Lysozyme Assay Kit (ThermoFisher Scientific). Micrococcus lysodeikticus cell walls (1 mg mL^{-1}, 100 μL) were mixed with the samples and incubated at 37 °C for 1 h in a light protected environment. The intact lysozyme lyses the bacterial cell wall and restores the fluorescence signal of FITC. Labeling of FITC with Micrococcus lysodeikticus cell walls causes the quenching of the fluorescent signal. The increase in fluorescent readings at 494 and 518 nm was proportional to the intact or activity of lysozyme. The data was normalized to the activity of the original activity of the lysozyme. All the analysis was performed on three independent experiments with two replicates.

Protein Stabilization Studies—Insulin Stabilization Assay: Solution of insulin (2 mg mL^{-1}) (Sigma–Aldrich) and all the stabilizing agents were prepared in glycine buffer (50 *m*M, pH 2.5) to a final concentration of 0.5 *m*M, for all. The efficiency of the stabilizing agents was measured by a thioflavin T fluorescence measurement assay.[20,83] Thioflavin T (ThT) was prepared in tris-buffer (10 *m*M, pH 8.0) to a concentration of 20 μM. Insulin forms fibrils upon heating and these fibrils react with Thioflavin which enhances the fluorescence. Insulin (100 μL) was mixed with 100 μL of stabilizing agent (or buffer) in a 2 mL glass vial and heated at 60 °C for 48 h. Fresh thioflavin T solution was prepared before each fluorescence measurement. Thioflavin T (20 μM, 190 μL) was mixed with 10 μL of the heated samples, centrifuged for 10 min. Then the samples were re-suspended using a pipette and fluorescence excitation and emission were measured at 450 and 486 nm respectively is shown in Figure S22 (Supporting Information). The data was normalized to the activity of the intact insulin that has never been heated. All the data are reported on three independent experiments (N = 3).

Protein Stabilization Studies—β-Galactosidase Stabilization Assay: The *β*- galactosidase (Sigma–Aldrich) solution (0.4 mg mL^{-1}) was prepared in sodium phosphate buffer (pH 7.0, 10 mM).[84] Three different concentrations of both stabilizing agents, HPOD-**2** and trehalose (4/2/0.4 mg mL^{-1}), were prepared in sodium phosphate buffer (pH 7.0, 10 mM). *O*-Nitrophenyl-*β*-galactoside (ONPG, Sigma–Aldrich) (1 mg mL^{-1}) was prepared in Mili-Q water and heated at 37 °C for 15 min to dissolve. *β*- Galactosidase (25 μL) was mixed with 75 μL of stabilizing agent in a 1.5 mL Eppendorf. All the samples were first frozen along with *β*-galactosidase alone by immersion in liquid nitrogen until all liquid appeared frozen (approximately for 5 min). The samples were lyophilized for two 4 h cycles and one-over-night cycle (15 h). After each cycle, 100 μL of Mili-Q water was added to each sample and again lyophilized. After the third cycle, 50 μL of Mili-Q water was added to all samples. ONPG solution (30 μL) was added to all samples and allowed to react in an environment devoid of light for 5 min. The intact *β*- galactosidase cleaves the ONPG, and generates a yellow compound (OD-420 nm). The reaction was then stopped with 50 μL of 1 M Na_2CO_3 solution and UV–vis absorption was read at 420 nm.

Protein Stabilization Studies—Preservation of Antibody Activity: Two polymers (HPOD-**2** and HPOD-**4**) and trehalose were used for the preservation of antibody function after three repeated freeze and thaw cycles (for every 24 h) and the analysis was performed using flow cytometry throughout 3 days. Anti A antibody (cat no: ab2521 [Abcam]) was mixed with each of trehalose (100 mg mL^{-1}), HPOD-**4** (100 mg mL^{-1}), and HPOD-**2** (100 mg mL^{-1}) in equal volumes and stored at −20 °C for further analysis. Antibody mixtures were then thawed daily (for three consecutive days) and incubated with 1% hematocrit A RBCs (1:500, RT, 30 min) that were collected after complete removal of platelet rich plasma (PRP) after centrifugation (Allegra X-22R centrifuge [Beckman Coulter]) of whole blood at 1000 g for 5 min to assess the antibody function. For detection of successful preservation of antibody function, a secondary Alexa Fluor 488-labelled antibody (goat anti-mouse IgM (heavy chain) cross-adsorbed secondary antibody, Alexa Fluor 488: cat no. A21042 [Invitrogen]) in a 1:300 concentration was applied at room temperature for 30 min and data were

collected using CytExpert Software 2.3 (Beckman Coulter) on a CytoFLEX flow cytometer. Fresh antibody aliquot that never went through freeze and thaw cycles was used as a control. 100% RBC population (10 000 counts) was used for flow cytometry assessment. To assure the purity of the cell population being assessed, naive RBCs were used to set a gate for the data collection. Data were collected only for the cell population defined by the gate. The following protocol was used for gating strategy. Naive RBCs at 1% hematocrit (were collected after centrifugation of whole blood at 1000 g for 5 min for the complete removal of PRP) were used to set a gate for the data collection. To confirm the cell population being assessed is RBCs, naive RBC samples were treated with 1/100 R-phycoerythrin (RPE)-conjugated monoclonal mouse anti-Human CD235a, Glycophorin A/RPE, Clone JC159 (cat no: R7078 [Dako]), at 4 °C for 30 min and assessed on a CytoFLEX flow cytometer [Beckman Coulter] to set a gate for the data collection. For "positive" antigen A expressing samples, blood group A was used, and for "negative" antigen A expressing samples, blood group O was used as controls. "Control" blood samples were typed using Micro Typing System (MTS) cards [ID-Micro Typing SystemTM (ID-MTSTM) Gel Cards from Ortho Clinical Diagnostics] according to the manufacturer's protocol prior to the flow cytometry assessment.

Mouse Tolerance Study—The Biocompatibility in Vivo Work was Conducted at the BC Cancer Agency; (Animal Ethics # A22-0274): Female Balb/cAnNHsd mice were purchased from Envigo and acclimated 7 days prior to study start. Mice were caged in autoclaved Allentown ventilated caging at a capacity of 4 animals/cage during the course of the experiment. Cages were changed bi-weekly. The mice were injected with one dose intravenously at 200 uL and returned to their cages. Therefore, the mice were individually weighed and injected with amount (polymer) per body weight (mouse) using HPOD solutions at 500, 250, 100, and 50 mg kg^{-1}, a PBS injection was used as controlled. There were 4 mice in each group and two sets were injected for short term and long-term toxicity. They were continually monitored for acute signs of toxicity for 2 h following each dose of test compound administration and clinical observations were monitored a minimum of once more at 6–8 h, then daily monitoring afterward. Upon termination after days 1 and 14 to test for acute and chronic toxicity, major organs (heart, spleen, kidneys, lungs, and liver) were harvested and stored in 10% normal buffered formalin. Blood samples were taken and the plasma was stored at −80 °C until further analysis. The organs were sectioned by Waxit Inc. (5 µm thick slices) and staining (haematoxylin and eosin stain). Histopathological analysis was performed at Vancouver General Hospital by the group of Prof. Dr. Caigan Du. Serum samples were analyzed with ALT and AST activity assay kit (Sigma Aldrich), and with LDH assay kit (abcam).

Mouse Tolerance Study—Ice Recrystallization Inhibition Studies: All the samples were prepared using 30 wt% sucrose solutions containing different polymers (HPOD-**4**, PVA (8 kDa) at 0.1, 1, and 10 mM and HES (180 kDa) at 0.1 and 1 mM). A droplet (0.5 µL) was added onto a microscope glass slide before pressing against another glass slide to create a film sealed by adding silicon grease along the edges. The space between two glass slides was kept consistent (≈160 µm thick) by using a small piece of aluminum foil as a spacer for all films prepared. The film was then placed onto a temperature-controlled flow cell coupled to an optical microscope (Axiolab; Zeiss, Oberkochen, Germany) with a CCD camera. The film was cooled to −50 °C to form small ice crystals (≈15 µm radii). Then, the film was heated to −9.1 °C, a temperature at which larger ice crystals grew at an appreciable rate at the expense of smaller ice crystals in the controls (i.e., no polymers). The temperature was held at this condition for 120 min. Digital images of the ice crystals were obtained using the optical microscope in transmission bright field mode every 10 min for 120 min. Images were analyzed using ImageJ software for crystal radius and reported as average ± standard deviation.

Statistical Analysis: Statistical analysis was performed using GraphPad Prism 9 (GraphPad Software, San Diego, USA). Pairwise multiple comparisons were conducted using unpaired t-test or ANOVA. Unless otherwise stated, all experiments were represented as average ± standard deviation of a minimum of three independent studies performed on different days.

Supporting Information

Supporting Information is available from the Wiley Online Library or from the author.

Acknowledgements

The authors acknowledge the funding from the Canadian Institutes of Health Research (CIHR), Canada Foundation for Innovation (CFI), and the Natural Science and Engineering Research Council of Canada (NSERC). The authors thank the Macromolecular Hub, Centre for Blood Research (CBR), for the use of their research facilities. JNK held a career investigator scholar award from the Michael Smith Foundation for Health Research (MSFHR). JNK is a Tier 1 Canada Research Chair in Immunomodulating Materials and Immunotherapy. AKB acknowledges a MSFHR Scholar award and a Tier II Canada Research Chair in Nucleic Acid Bioengineering. AH acknowledges Michael Smith Health Research BC and Deutsche Forschungsgemeinschaft (DFG) postdoctoral fellowship. SA acknowledges a MSFHR postdoctoral fellowship. NVB acknowledges an NMIN Graduate award and NSERC CREATE CITF program, UA a graduate scholarship from CBR. HM, AG, and HDL acknowledge the funding from NSERC CREATE NanoMat Program. HM and HDL are further supported by Canadian Blood Services-MITACS fellowship and NSERC CGS-M fellowship respectively. EA acknowledges a summer studentship program fellowship from CBR.

Conflict of Interest

The University of British Columbia has filed a patent application based on the data provided with J.N.K., A.H., S.A., and A.K.B. as inventors. No conflicts with other authors.

Author Contributions

A.H. and S.A. contributed equally to this work. A.H. designed and performed the LNP preservation studies and identified lead compounds. S.A. designed, performed initial synthesis, characterized HPODs, and identified the hydration characteristics. IC synthesized and characterized HPODs. PMMN helped in characterization. U.A. and A.G. synthesized and characterized HPODs. A.K.B. and N.V.B. did the in vivo LNP studies and provided saRNA-LNPs. E.A., S.A., and H.M. performed protein preservation studies. A.H and M.D. did the biocompatibility studies. CD did the histology assessment. HDL worked on ice recrystallization inhibition studies, and Y.X. and A.B. assisted in analyzing data. PM helped with polymer characterization and mass spectrometry data. RH developed and provided polyglycerol dendrimer. The manuscript was written by A.H., S.A., and J.N.K. with the help of other co-authors. All authors contributed to the editing of the manuscript. A.K.B. designed experiments, provided supervision and grant support for the project. J.N.K. conceived the project, designed experiments, provided supervision and grant support for the project.

Data Availability Statement

The data that support the findings of this study are available in the supplementary material of this article.

Keywords

cryopreservation, heat stabilization, lyophilization, mRNA/saRNA lipid nanoparticles, polymer topology, protein therapeutics, universal polymer excipient

Received: April 22, 2024
Revised: July 15, 2024
Published online: August 1, 2024

[1] N. Chennamsetty, V. Voynov, V. Kayser, B. Helk, B. L. Trout, *Proc. Natl. Acad. Sci* **2009**, *106*, 11937.
[2] B. Leader, Q. J. Baca, D. E. Golan, *Nat. Rev. Drug Discovery* **2008**, *7*, 21.
[3] N.-N. Zhang, X.-F. Li, Y.-Q. Deng, H. Zhao, Y.-J. Huang, G. Yang, W.-J. Huang, P. Gao, C. Zhou, R.-R. Zhang, Y. Guo, S.-H. Sun, H. Fan, S.-L. Zu, Q. Chen, Q. He, T.-S. Cao, X.-Y. Huang, H.-Y. Qiu, J.-H. Nie, Y. Jiang, H.-Y. Yan, Q. Ye, X. Zhong, X.-L. Xue, Z.-Y. Zha, D. Zhou, X. Yang, Y.-C. Wang, B. Ying, et al., *Cell* **2020**, *182*, 1271.
[4] M. H. Y. Cheng, C. A. Brimacombe, R. Verbeke, P. R. Cullis, *Mol. Pharmaceutics* **2022**, *19*, 1663.
[5] S. Bevers, S. A. A. Kooijmans, E. Van de Velde, M. J. W. Evers, S. Seghers, J. J. J. M. Gitz-Francois, N. C. H. van Kronenburg, M. H. A. M. Fens, E. Mastrobattista, L. Hassler, H. Sork, T. Lehto, K. E. Ahmed, S. El Andaloussi, K. Fiedler, K. Breckpot, M. Maes, D. Van Hoorick, T. Bastogne, R. M. Schiffelers, S. De Koker, *Mol. Ther.* **2022**, *30*, 3078.
[6] Y. Eygeris, S. Patel, A. Jozic, G. Sahay, *Nano Lett.* **2020**, *20*, 4543.
[7] D. Zhang, G. Wang, X. Yu, T. Wei, L. Farbiak, L. T. Johnson, A. M. Taylor, J. Xu, Y. Hong, H. Zhu, D. J. Siegwart, *Nat. Nanotechnol.* **2022**, *17*, 777.
[8] J. B. Miller, S. Zhang, P. Kos, H. Xiong, K. Zhou, S. S. Perelman, H. Zhu, D. J. Siegwart, *Angew. Chem., Int. Ed.* **2017**, *56*, 1059.
[9] L. Schoenmaker, D. Witzigmann, J. A. Kulkarni, R. Verbeke, G. Kersten, W. Jiskoot, D. J. A. Crommelin, *Int. J. Pharm.* **2021**, *601*, 120586.
[10] S. Frokjaer, D. E. Otzen, *Nat. Rev. Drug Discovery* **2005**, *4*, 298.
[11] S. Mitragotri, P. A. Burke, R. Langer, *Nat. Rev. Drug Discovery* **2014**, *13*, 655.
[12] T. Arakawa, S. J. Prestrelski, W. C. Kenney, J. F. Carpenter, *Adv. Drug Del. Rev.* **2001**, *46*, 307.
[13] B. A. Kerwin, *J. Pharm. Sci.* **2008**, *97*, 2924.
[14] K. Shiraishi, M. Yokoyama, *Sci Technol Adv Mat* **2019**, *20*, 324.
[15] B. Panganiban, B. Qiao, T. Jiang, C. DelRe, M. M. Obadia, T. D. Nguyen, A. A. A. Smith, A. Hall, I. Sit, M. G. Crosby, P. B. Dennis, E. Drockenmuller, M. Olvera de la Cruz, T. Xu, *Science* **2018**, *359*, 1239.
[16] Y. Liu, J. Lee, K. M. Mansfield, J. H. Ko, S. Sallam, C. Wesdemiotis, H. D. Maynard, *Bioconjugate Chem.* **2017**, *28*, 836.
[17] B. Marco-Dufort, J. R. Janczy, T. Hu, M. Lütolf, F. Gatti, M. Wolf, A. Woods, S. Tetter, B. V. Sridhar, M. W. Tibbitt, *Sci. Adv.* **2022**, *8*, eabo0502.
[18] D. E. Pegg, *Semin Reprod Med* **2002**, *20*, 005.
[19] F. C. Herbert, S. S. Abeyrathna, N. S. Abeyrathna, Y. H. Wijesundara, O. R. Brohlin, F. Carraro, H. Amenitsch, P. Falcaro, M. A. Luzuriaga, A. Durand-Silva, S. D. Diwakara, R. A. Smaldone, G. Meloni, J. J. Gassensmith, *Nat. Commun.* **2021**, *12*, 2202.
[20] R. J. Mancini, J. Lee, H. D. Maynard, *J. Am. Chem. Soc.* **2012**, *134*, 8474.
[21] C. I. Biggs, T. L. a. Bailey, *Nat. Commun.* **2017**, *8*, 1546.
[22] F. M. Coyle, S. J. S. J. Martin, V. J. McBrierty, *J. Mol. Liq.* **1996**, *69*, 95.
[23] R. M. Hodge, G. H. Edward, G. P. Simon, *Polymer* **1996**, *37*, 1371.
[24] A. J. Keefe, S. Jiang, *Nat. Chem.* **2012**, *4*, 59.
[25] M. Griffith, K. V. Ewart, *Biotechnol. Adv.* **1995**, *13*, 375.
[26] T. H. Nguyen, S.-H. H. Kim, C. G. Decker, D. Y. Wong, J. A. Loo, H. D. Maynard, *Nat. Chem.* **2013**, *5*, 221.
[27] E. Papakonstantinou, M. Roth, G. Karakiulakis, *Dermato-Endocrinology* **2012**, *4*, 253.
[28] E. Oude Blenke, E. Örnskov, C. Schöneich, G. A. Nilsson, D. B. Volkin, E. Mastrobattista, Ö. Almarsson, D. J. A. Crommelin, *J. Pharm. Sci.* **2023**, *112*, 386.
[29] S. Ohtake, Y. J. Wang, *J. Pharm. Sci.* **2011**, *100*, 2020.
[30] D. E. Mitchell, A. E. R. Fayter, R. C. Deller, M. Hasan, J. Gutierrez-Marcos, M. I. Gibson, *Mater. Horiz.* **2019**, *6*, 364.
[31] S. Y. Lee, M. Kim, T. K. Won, S. H. Back, Y. Hong, B.-S. Kim, D. J. Ahn, *Nat. Commun.* **2022**, *13*, 6532.
[32] S. Abbina, S. Vappala, P. Kumar, E. M. J. Siren, C. C. La, U. Abbasi, D. E. Brooks, J. N. Kizhakkedathu, *J. Mater. Chem. B* **2017**, *5*, 9249.
[33] R. K. Kainthan, J. Janzen, E. Levin, D. V. Devine, D. E. Brooks, *Biomacromolecules* **2006**, *7*, 703.
[34] J. K. Armstrong, R. B. Wenby, H. J. Meiselman, T. C. Fisher, *Biophys. J.* **2004**, *87*, 4259.
[35] A. Sunder, R. Hanselmann, H. Frey, R. Mülhaupt, *Macromolecules* **1999**, *32*, 4240.
[36] D. Hölter, A. Burgath, H. Frey, *Acta Polym.* **1997**, *48*, 30.
[37] D. Wilms, J. Nieberle, J. Klos, H. Löwe, H. Frey, *Chem. Eng. Technol.* **2007**, *30*, 1519.
[38] D. Kosyakov, O. Khoroshev, E. Anikeenko, N. Ul'yanovskii, *J. Anal. Chem.* **2019**, *74*, 1382.
[39] R. Haag, A. Sunder, J. F. Stumbé, *J. Am. Chem. Soc.* **2000**, *122*, 2954.
[40] C. Du, A. A. Mendelson, Q. Guan, R. Chapanian, I. Chafeeva, G. da Roza, J. N. Kizhakkedathu, *Biomaterials* **2014**, *35*, 1378.
[41] L. R. Winther, J. Qvist, B. Halle, *J. Phys. Chem. B* **2012**, *116*, 9196.
[42] A. Wolde-Kidan, A. Herrmann, A. Prause, M. Gradzielski, R. Haag, S. Block, R. R. Netz, *Biophys. J.* **2021**, *120*, 463.
[43] A. Akinc, M. A. Maier, M. Manoharan, K. Fitzgerald, M. Jayaraman, S. Barros, S. Ansell, X. Du, M. J. Hope, T. D. Madden, B. L. Mui, S. C. Semple, Y. K. Tam, M. Ciufolini, D. Witzigmann, J. A. Kulkarni, R. van der Meel, P. R. Cullis, *Nat. Nanotechnol.* **2019**, *14*, 1084.
[44] A. K. Blakney, P. Deletic, P. F. McKay, C. R. Bouton, M. Ashford, R. J. Shattock, A. Sabirsh, *J. Controlled Release* **2021**, *330*, 1250.
[45] P. F. McKay, K. Hu, A. K. Blakney, K. Samnuan, J. C. Brown, R. Penn, J. Zhou, C. R. Bouton, P. Rogers, K. Polra, P. J. C. Lin, C. Barbosa, Y. K. Tam, W. S. Barclay, R. J. Shattock, *Nat. Commun.* **2020**, *11*, 3523.
[46] X. Hou, T. Zaks, R. Langer, Y. Dong, *Nat. Rev. Mater.* **2021**, *6*, 1078.
[47] K. J. Hassett, J. Higgins, A. Woods, B. Levy, Y. Xia, C. J. Hsiao, E. Acosta, Ö. Almarsson, M. J. Moore, L. A. Brito, *J. Controlled Release* **2021**, *335*, 237.
[48] J. Di, Z. Du, K. Wu, S. Jin, X. Wang, T. Li, Y. Xu, *Pharm. Res.* **2022**, *39*, 105.
[49] G. Guerrini, D. Magrì, S. Gioria, D. Medaglini, L. Calzolai, *Nat. Nanotechnol.* **2022**, *17*, 570.
[50] Y. Suzuki, H. Ishihara, *Drug Metab. Pharmacokinet.* **2021**, *41*, 100424.
[51] C. Olsson, J. Swenson, *J. Phys. Chem. B* **2020**, *124*, 3074.
[52] A. K. Blakney, P. F. McKay, K. Hu, K. Samnuan, N. Jain, A. Brown, A. Thomas, P. Rogers, K. Polra, H. Sallah, J. Yeow, Y. Zhu, M. M. Stevens, A. Geall, R. J. Shattock, *J. Controlled Release* **2021**, *338*, 201.
[53] L. Ai, Y. Li, L. Zhou, W. Yao, H. Zhang, Z. Hu, J. Han, W. Wang, J. Wu, P. Xu, R. Wang, Z. Li, Z. Li, C. Wei, J. Liang, H. Chen, Z. Yang, M. Guo, Z. Huang, X. Wang, Z. Zhang, W. Xiang, D. Sun, L. Xu, M. Huang, B. Lv, P. Peng, S. Zhang, X. Ji, H. Luo, et al., *Cell Discov.* **2023**, *9*, 9.
[54] H. Muramatsu, K. Lam, C. Bajusz, D. Laczkó, K. Karikó, P. Schreiner, A. Martin, P. Lutwyche, J. Heyes, N. Pardi, *Mol. Ther.* **2022**, *30*, 1941.
[55] R. L. Ball, P. Bajaj, K. A. Whitehead, *Int J Nanomedicine* **2017**, *12*, 305.
[56] W. Wang, *Protein Sci.* **2015**, *24*, 1031.
[57] K. A. Pikal-Cleland, N. Rodrguez-Hornedo, G. L. Amidon, J. F. Carpenter, *Arch. Biochem. Biophys.* **2000**, *384*, 398.
[58] J. Lee, E.-W. Lin, U. Y. Lau, J. L. Hedrick, E. Bat, H. D. Maynard, *Biomacromolecules* **2013**, *14*, 2561.
[59] H. Kawai, M. Sakurai, Y. Inoue, R. Chuj, S. Kobayashi, *Cryobiology* **1992**, *29*, 599.
[60] C. Budke, A. Dreyer, J. Jaeger, K. Gimpel, T. Berkemeier, A. S. Bonin, L. Nagel, C. Plattner, A. L. DeVries, N. Sewald, T. Koop, *Cryst. Growth Des.* **2014**, *14*, 4285.
[61] R. C. Deller, M. Vatish, D. A. Mitchell, M. I. Gibson, *Nat. Commun.* **2014**, *5*, 3244.
[62] D. E. Mitchell, J. R. Lovett, S. P. Armes, M. I. Gibson, *Angew. Chem., Int. Ed.* **2016**, *55*, 2801.

[63] M. L. Brader, S. J. Williams, J. M. Banks, W. H. Hui, Z. H. Zhou, L. Jin, *Biophys. J.* **2021**, *120*, 2766.
[64] P. Patel, N. M. Ibrahim, K. Cheng, *Trends Pharmacol. Sci.* **2021**, *42*, 448.
[65] J. H. Ko, H. D. Maynard, *Chem. Soc. Rev.* **2018**, *47*, 8998.
[66] R. G. Strickley, W. J. Lambert, *J. Pharm. Sci.* **2021**, *110*, 2590.
[67] J. K. Kaushik, R. Bhat, *J. Biol. Chem.* **2003**, *278*, 26458.
[68] B. P. Best, *Rejuvenation Research* **2015**, *18*, 422.
[69] B. S. Bhatnagar, R. H. Bogner, M. J. Pikal, *Pharm. Dev. Technol.* **2007**, *12*, 505.
[70] K. A. Murray, M. I. Gibson, *Nat. Rev. Chem.* **2022**, *6*, 579.
[71] R. Chapanian, I. Constantinescu, N. A. A. Rossi, N. Medvedev, D. E. Brooks, M. D. Scott, J. N. Kizhakkedathu, *Biomaterials* **2012**, *33*, 7871.
[72] P. Czechura, R. Y. Tam, E. Dimitrijevic, A. V. Murphy, R. N. Ben, *J. Am. Chem. Soc.* **2008**, *130*, 2928.
[73] A. Sunder, R. Hanselmann, H. Frey, R. Mlhaupt, *Macromolecules* **1999**, *32*, 4240.
[74] M. I. Ul-haq, R. A. Shenoi, D. E. Brooks, J. N. Kizhakkedathu, *J. Polym. Sci., Part A: Polym. Chem.* **2013**, *51*, 2614.
[75] A. Sunder, H. Türk, R. Haag, H. Frey, *Macromolecules* **2000**, *33*, 7682.
[76] M. Imran ul-haq, B. F. L. Lai, R. Chapanian, J. N. Kizhakkedathu, *Biomaterials* **2012**, *33*, 9135.
[77] P. Anilkumar, T. B. Lawson, S. Abbina, J. T. A. Mäkelä, R. C. Sabatelle, L. E. Takeuchi, B. D. Snyder, M. W. Grinstaff, J. N. Kizhakkedathu, *Nat. Commun.* **2020**, *11*, 2139.
[78] W. S. Price, *Concepts Magn. Reson.* **1997**, *9*, 299.
[79] J. A. Kulkarni, D. Witzigmann, S. Chen, P. R. Cullis, R. van der Meel, *Acc. Chem. Res.* **2019**, *52*, 2435.
[80] H. H. Ly, S. Daniel, S. K. V. Soriano, Z. Kis, A. K. Blakney, *Mol. Pharmaceutics* **2022**, *19*, 1892.
[81] I. C. Casmil, C. Huang, A. K. Blakney, *Sci. Rep.* **2023**, *13*, 19050.
[82] A. K. Blakney, P. F. McKay, D. Christensen, B. I. Yus, Y. Aldon, F. Follmann, R. J. Shattock, *J. Controlled Release* **2019**, *304*, 65.
[83] S. Vilasi, C. Iannuzzi, M. Portaccio, G. Irace, I. Sirangelo, *Biochemistry* **2008**, *47*, 1789.
[84] C. Xue, T. Y. Lin, D. Chang, Z. Guo, *R. Soc. Open Sci.* **2017**, *4*, 160696.